DOI:10.14753/SE.2017.2028

Timing of motions in the CFTR channel protein during pore opening

Ph.D. Doctoral Dissertation

Dr. Ben Sorum

Molecular Medicine Doctoral School

Semmelweis University

Supervisor: Dr. László Csanády M.D., D.Sc.

Official Reviewers:
Dr. György Panyi M.D., D.Sc.
Dr. Péter Várnai M.D., Ph.D.

Head of the Final Examination Committee:
Dr. Csala Miklós Ph.D.

Members of the Final Examination Committee:
Dr. Keszler Gergely Ph.D.
Dr. Flóra Szeri Ph.D.

Budapest
2017

DOI:10.14753/SE.2017.2028

Table of Contents

DOI:10.14753/SE.2017.2028

DOI:10.14753/SE.2017.2028

List of Abbreviations

ABC.....ATP binding cassette

ADP.....adenosine diphosphate

ATP.....adenosine triphosphate

CF.....cystic fibrosis

CFTR.....cystic fibrosis transmembrane conductance regulator

CH..... coupling helix

ΔF..... phenylalanine deletion

ICL.....intracellular loop

K_{eq}.....equilibrium constant

k_{co}.....opening rate

k_{oc}.....closing rate

NBD.....nucleotide binding domain

P_c.....closed probability

P-gp.....P-glycoprotein

PKA.....protein kinase A

P_o.....open probability

R.....regulatory domain

REFER.....rate-equilibrium free energy relationship

τ_b.....mean burst duration

τ_{ib}.....mean interburst duration

TMD.....transmembrane domain

$T^{\ddagger}$.....transition state

DOI:10.14753/SE.2017.2028

1. Introduction

1.1. Role of CFTR in health and disease

The cystic fibrosis transmembrane conductance regulator (CFTR) is a chloride ion channel expressed at the apical surfaces of various epithelial layers, including the lung, intestinal mucosa, exocrine pancreas, vas deferens, and the sweat duct, and its function is essential for the salt-water balance of these surfaces under physiological conditions.

Cystic fibrosis (CF), caused by dysfunction of CFTR due to mutations, is the most common lethal genetic disease in Caucasian populations[1], with a frequency of ~1/2500. CF is a destructive multiorgan disorder, which presents with blockage of airway passages due to viscous mucus, frequent respiratory infections, obstruction of pancreatic ducts, meconium ileus in newborn, infertility in males due to blockage of the vas deferens, as well as a distinctive high-salt sweat which is diagnostic for the disease. Even though in recent decades progress in symptomatic treatment has greatly extended the life expectancy of CF patients, the most common form of the disease remains incurable to date. On the other hand, overactive CFTR kept in a constitutively stimulated state due to the action of bacterial toxins, mediates fluid loss into the intestinal lumen in secretory diarrheas such as cholera, still very frequent in developing countries[2].

CFTR belongs to the ATP binding cassette (ABC) protein superfamily, whose members are involved in a broad variety of physiological, pharmacological and pathological processes[3]. Although ABC proteins are active transporters whereas CFTR, alone, is a chloride ion channel, recent results suggest that a conserved molecular mechanism couples a cycle of conformational changes between cytosolic nucleotide binding domains (NBDs) and transmembrane domains (TMDs) of all ABC proteins[4].

1.2. ABC transporters and their general structure

ABC transporters are members of a transport system superfamily that is arguably one of the largest and most ancient transporter families, with representatives in all existing phyla from prokaryotes to homo sapiens[5, 6]. From the current sequence information of microbial genomes, ABC transporters represent the largest protein

family identified up until now; underlined by the fact that between one and three percent of bacterial and archaeal genomes encode for subunits of ABC transporters[6]. Forty eight ABC transporters are known to exist in humans[7, 8], and a large number of these have revealed to be responsible for, or associated with, various disease states, including (but not limited to) adrenoleukodystrophy, neonatal diabetes, Tangier disease, pseudoxanthoma elasticum, and CF[9].

The general structural make-up of every ABC transporter is composed of two types of modular domains: the transmembrane domain (TMD) and the nucleotide binding domain (NBD). The TMD, also known as membrane-spanning domain or integral membrane domain, is made up of alpha helices, traversing the membrane bilayer[10]. It normally recognizes an assortment of substrates, and goes through conformational transformations between inward-facing and outward-facing states that alternately expose the substrate binding sites to the two sides, to transport such substrates across the membrane[10]. Correspondingly, the sequence and architecture of TMDs is highly variable, reflecting the chemical diversity of substrates that can be translocated[10]. The NBD on the other hand, is located in the cytoplasm, and is the site for ATP binding and hydrolysis, required for driving unidirectional, thermodynamically uphill, transport[10]. Correspondingly, NBD sequences are highly conserved, and form an ABC consisting of two subdomains, a core ("head") and an α-helical ("tail") subdomain. ATP binds to the highly conserved Walker A (GXXXXKT/S) and B (ΦΦΦΦDE, Φ hydrophobic) motifs of the core subdomain, present in most ATPases, whereas a third highly conserved motif, the ABC signature sequence (LSGGQR/K) is found in the α-helical subdomain, distant from bound ATP[11, 12].

With a few exceptions, most functional ABC transporters contain two TMDs and two NBDs, which may be expressed from a variable number of genes. In several bacterial importers the four canonical domains are expressed as individual polypeptides and coassemble with each other into a functional protein. In most bacterial exporters, an N-terminal TMD is fused to a C-terminal NBD, and two such "half-transporters" assemble into homo- or heterodimers. Human ABC transporters are expressed either as half-transporters, or fused into a single polypeptide chain, and are typically arranged in the following order: TMD1-NBD1-TMD2-NBD2 (*Figure 1.*).

DOI:10.14753/SE.2017.2028

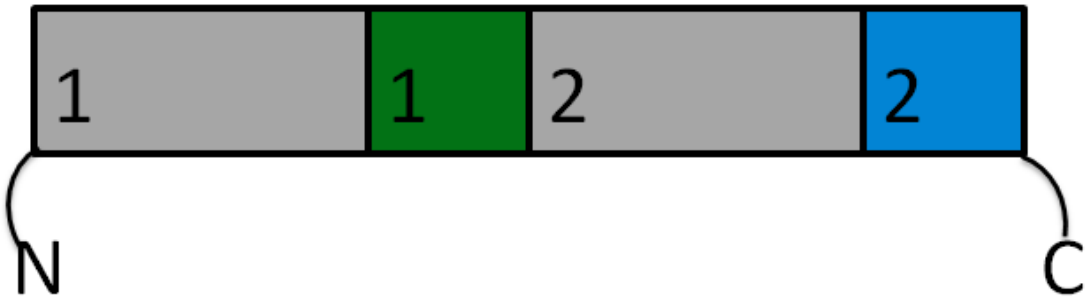

Figure 1. Modular architecture of ABC proteins

Typical sequential arrangement of the four canonical ABC domains in monomeric ABC proteins. From left to right: the N-terminus, TMD1 (gray rectangle 1), NBD1 (green box 1), TMD2 (gray rectangle 2), NBD2 (blue box 2).

1.2.1. Crystal structures of ABC transporters

The latest developments in X-ray crystallographic determination of an array of bacterial and eukaryotic ABC transporter structures have helped to advance our understanding of the ATP hydrolysis-driven transport mechanism, but have also depicted the huge structural and functional diversity within the family[4]. Numerous intermediate to high resolution crystal structures have been resolved for many ABC transporters that range from microorganisms to higher eukaryotes, including mammals. These detailed structural data, combined with comprehensive biochemical and biophysical studies, have given us a wealth of information on the catalytic process of ATP hydrolysis-driven transport[9].

1.2.1.1. Crystal structure of Sav1866

The first high-resolution structure reported for a full-length ABC exporter was that of the multidrug exporter Sav1866 from *Staphylococcus aureus*.[13, 14]. The NBDs of the Sav1866 homodimer are similar in structure to those of other ABC transporters. They expose conserved motifs involved in ATP binding and hydrolysis[15] at the shared interface of a ‘head-to-tail’ dimeric arrangement that has been widely accepted as physiologically relevant on the basis of structural[16, 17] and biochemical[18-20] data. The hallmark of this NBD dimer arrangement is that two ATP-binding sites are formed at the shared interface, formed on one side by the Walker-A (also called the P-loop) and Walker B motifs of one NBD, and on the other side by the ABC signature motif of the opposing NBD. Involvement of both NBDs in the formation of both binding sites creates a direct link between the two sites and provides the molecular basis of the observed cooperativity in ATP binding and hydrolysis[21]. The Sav1866 protein was crystallized in the presence of adenosine diphosphate (ADP), and two ADP molecules were resolved in the structure, both buried inside the dimer between the P-loops and the ABC signature motifs of opposing NBD subunits. Although ADP, rather than ATP, was bound, the NBDs in Sav1866 exhibit the tightly dimerized conformation expected for the ATP-bound state based on biochemical studies[22, 23]. At the same time, the TMDs were seen to adopt an outward-facing conformation with an unexpected twist that puts intracellular loops of both TMDs into contact with the membrane-facing surfaces of both NBDs ("domain-swap" arrangement)[24].

The structure further identified a short "coupling helix" (CH) in each of the four intracellular loops[24]. These helices run in parallel with the cytoplasmic face of the membrane, and were proposed to act as linkers between TMD and NBD domains, transmitting conformational movements between them[24].

In addition to the wealth of new information on ABC transporter structure and mechanism relevant to the entire ABC field, the Sav1866 structure provided the first clue for understanding the molecular consequences of the most common CF causing mutation, deletion of phenylalanine 508 in CFTR's NBD1. When aligned with the Sav1866 sequence, this CFTR residue maps to a conserved aromatic cluster of aminoacids on the NBD surface that is seen to contact a similar cluster of aromatic residues in and around CH2 in the Sav structure. Due to the domain-swap arrangement, the F508 residue in CFTR is predicted to contact CH4, which is part of the TMD2 sequence. The ΔF508 mutation, responsible for ~90% of CF cases, was therefore predicted to disrupt the normal domain-domain interaction at the NBD-TMD interface.

1.2.1.2. Crystal structure of TM287-288

Whereas in most ABC proteins both catalytic sites are hydrolytically active, a subset of the superfamily – including the entire C subfamily into which CFTR belongs – exhibits only one catalytically active site, while the other contains non-canonical substitutions in key conserved motifs and is therefore inactive[25]. The first crystal structure to be solved for such an "asymmetrical" ABC protein was that of TM287/288 from *Thermotoga maritima*, a heterodimeric ABC exporter with nonequal ATP binding sites[25]. The high-resolution (2.9-Å) TM287-288 structure is in its intracellular-facing conformation[25], and – similar to available intracellular-facing structures of symmetrical ABC proteins[26, 27]– its NBDs are disconnected from each other, revealing the nucleotide binding sites to the cytoplasmic milieu. This NBD boundary disconnection is accompanied by an increase, compared to that seen in Sav1866, in the distances between all four of the CHs, likely responsible for separating the cytoplasmic ends of the TM helices apart. However, in contrast to inward-facing symmetrical ABC exporter structures in some of which the two NBDs are seen wide apart, the NBDs of TM287-288 only partially separate, retaining some contact across the degenerate binding site, through an interface that involves the P-loop on one side, and the

conserved "D-loop" (following the Walker B motif) on the other. Based on the TM287-288 structure, a 15-Å separation of the coupling helices of ICL2 and ICL4 is sufficient to cause the TMDs to flip from an outward- to an inward-facing conformation, without the need for complete NBD dimer disengagement.

1.2.2. CFTR structure

CFTR is a monomeric ABC protein[28] built from two homologous halves, each comprising a TMD (*Figure 2., gray*) followed by a cytosolic NBD (*Figure 2, green and blue*), but is unique in that its TMDs form an chloride-selective transmembrane ion channel[29]. Both TMDs are built from six transmembrane α-helices (TM1-12), and extensive functional studies have identified TM1, 6, 11, and 12 to be involved in forming its anion-selective ion permeation pathway[30-37]. In CFTR, the two canonical ABC halves (TMD1-NBD1 and TMD2-NBD2) are linked into a single polypeptide by the unique cytosolic regulatory (R) domain (*Figure 2., pink*), resulting in the following sequential domain order: TMD1-NBD1-R-TMD2-NBD2.

The R domain is unrelated in its sequence to any other known protein, and is a target for phosphorylation by cAMP-dependent protein kinase (protein kinase A, PKA)[28] at multiple serine residues[38]. R-domain phosphorylation is a prerequisite for ATP-driven CFTR chloride channel activity[39](*Figure 3.*).

The structures of the isolated NBD1[41] and NBD2 (PDBID: 3GD7) domains of CFTR follow the conserved ABC NBD fold. However, to date, a detailed understanding of CFTR structure and function is limited by the lack of a full-length CFTR crystal structure. Consequently, several homology models of closed- and open-state CFTR have been constructed based on crystal structures of homologous ABC exporters in their inward- and outward-facing conformations ([42],[40]). (*Figure 4.*)

DOI:10.14753/SE.2017.2028

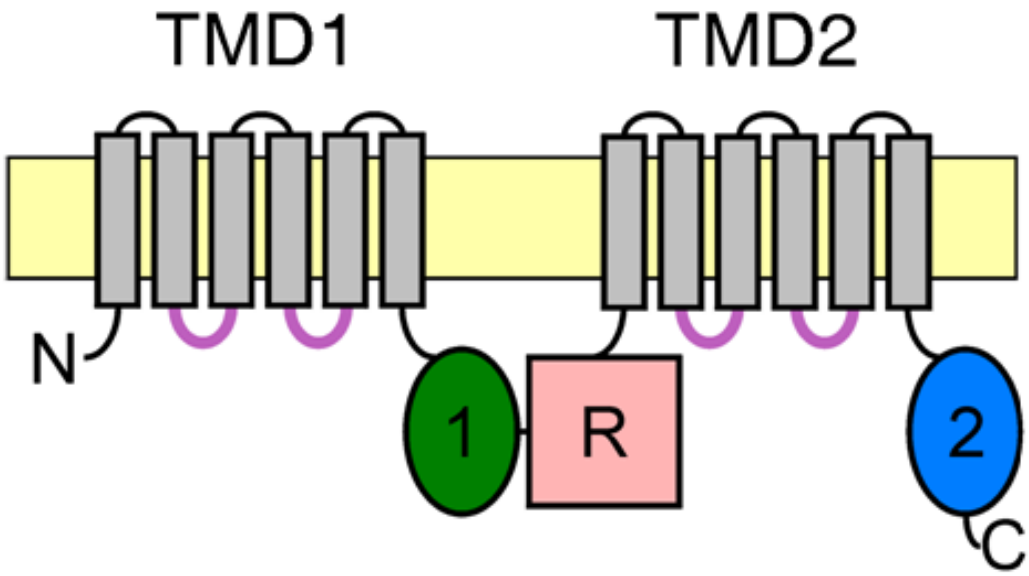

Figure 2. CFTR membrane topology

Domain organizations of WT CFTR: TMDs (gray), intracellular loops (ICLs) containing coupling helices (light violet), NBD1 (green), NBD2 (blue), R domain (pink), membrane (yellow).

DOI:10.14753/SE.2017.2028

Figure 3. Regulation of CFTR channel gating by PKA and ATP

CFTR's R domain must be phosphorylated by PKA before ATP is able to support channel opening. Current recording of a single wild-type CFTR channel in an inside-out membrane patch obtained in symmetrical 140 mM chloride, at a membrane potential of -80 mV. Downward deflections reflect individual pore opening events. The channel is activated by exposure to 300 nM catalytic subunit of bovine PKA (red bar) in the presence of 2 mM MgATP (green bar). On PKA withdrawal endogenous membrane-attached phosphatases partly dephosphorylate the R domain, thereby reducing the probability of finding the channel open, but channels do not stop gating until ATP is removed.

DOI:10.14753/SE.2017.2028

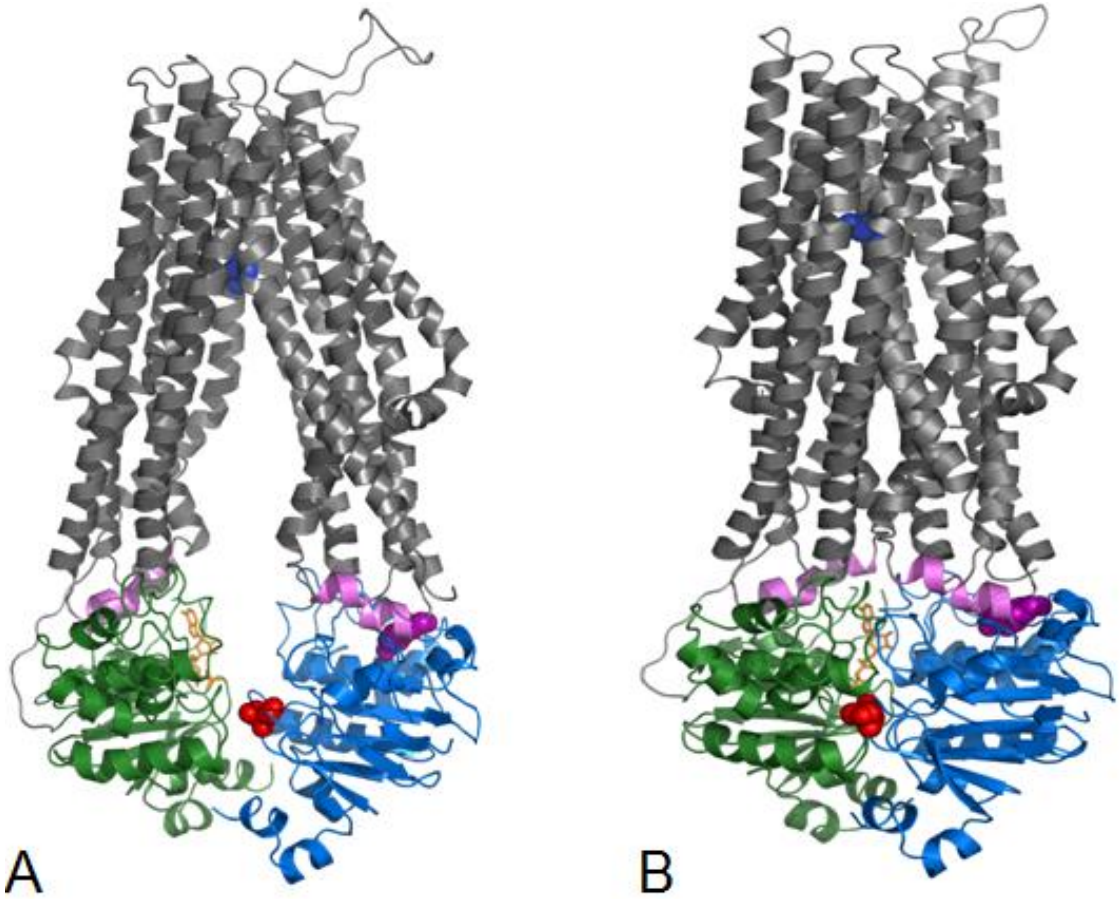

Figure 4. CFTR homology models

Ribbon representation of CFTR homology models[40] in the closed (A) and open (B) states based on (A) the inward-facing structure of TM287-288[25] and (B) the outward-facing structure of Sav1866[24].CFTR domain color coding follows that in Figure 2.; due to lack of a structural template, the R domain is omitted from the homology models. Three amino acid positions are highlighted in spacefill: threonine 1246 (red) located within NBD2, tyrosine 275 (violet) located at the TMD-NBD interface, and methionine 348 (blue) located within the pore.

DOI:10.14753/SE.2017.2028

1.3. ABC protein functional cycle

In ABC proteins, ATP binding triggers association of the two NBDs into a stable head-to-tail dimer that occludes two molecules of ATP (*Figure 5.A, yellow sticks*) at the interface[17]. By forming strong interactions with conserved residues of both the Walker motifs in the head of one NBD and the signature sequence in the tail of the opposing NBD these ATP molecules act as molecular glue that ties the NBDs together, and prompt dimer disruption therefore requires ATP hydrolysis[43]. Consequently, disrupting ATP hydrolysis by catalytic site mutations, such as substitutions of the presumed catalytic base (the glutamate residue at the end of the Walker B sequence), trap ABC NBDs in this tightly dimerized state. Based on full-length transporter structures (see 1.2.1.1. and 1.2.1.2.) NBD dimer formation is believed to be the trigger that flips the TMDs from an inward- (*Figure 6., left states*) to an outward-facing (*Figure 6., right states*) orientation, while dimer disruption following ATP hydrolysis and substrate release resets them to inward-facing. As discussed above, NBD-to-TMD signal transmission is likely mediated by an interface that includes the four short coupling helices (CH1–4)[4] in the four TMD intracellular loops (cf., *Figure 4., violet helices*).

DOI:10.14753/SE.2017.2028

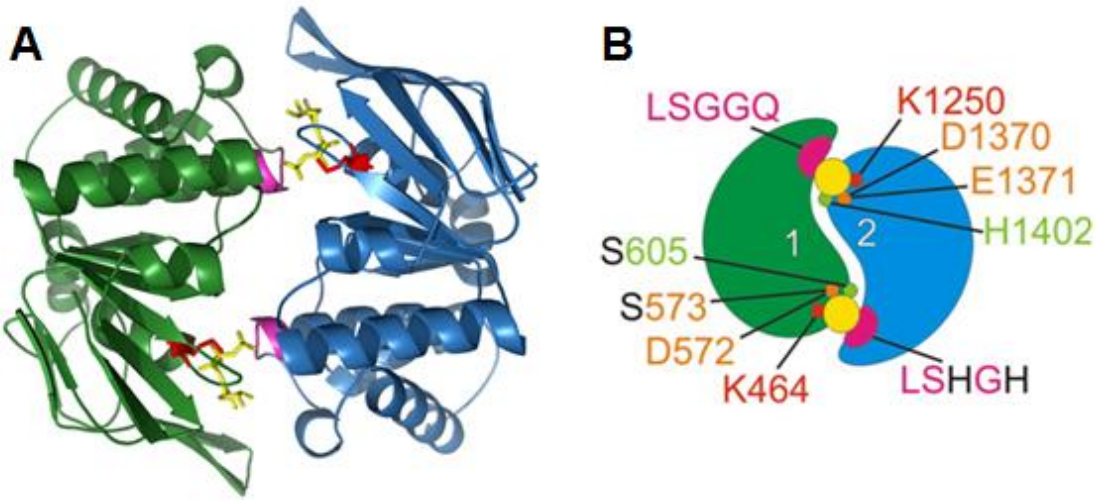

Figure 5. NBD dimer architecture

A, Ribbon representation of the structure (PDBID: 1L2T) of the Mj0796 ATP binding cassette from Methanococcus jannaschii trapped in an ATP-bound dimerized state due to mutation of the catalytic glutamate. ATP (yellow sticks) is sandwiched between the two NBDs (green and blue), and seen to form contacts with opposing Walker A lysines (red sticks) and residues of the signature motif (magenta).

B, Cartoon representation of the CFTR NBD1-NBD2 heterodimer. NBD1 is in green, NBD2 is in blue, ATP molecules are represented by yellow spheres. Key NBD2 head residues K1250 (Walker A), D1370 and E1371 (Walker B), and H1402 ("switch" histidine), are depicted as small colored spheres. Analogous positions in the NBD1 head follow the same color coding. Signature sequences in both NBD "tail" regions are also depicted. Note replacement by serines of the Walker B glutamate and of the switch histidine in the NBD1 head, as well as non-canonical substitutions (black letters) in the NBD2-tail signature sequence..

DOI:10.14753/SE.2017.2028

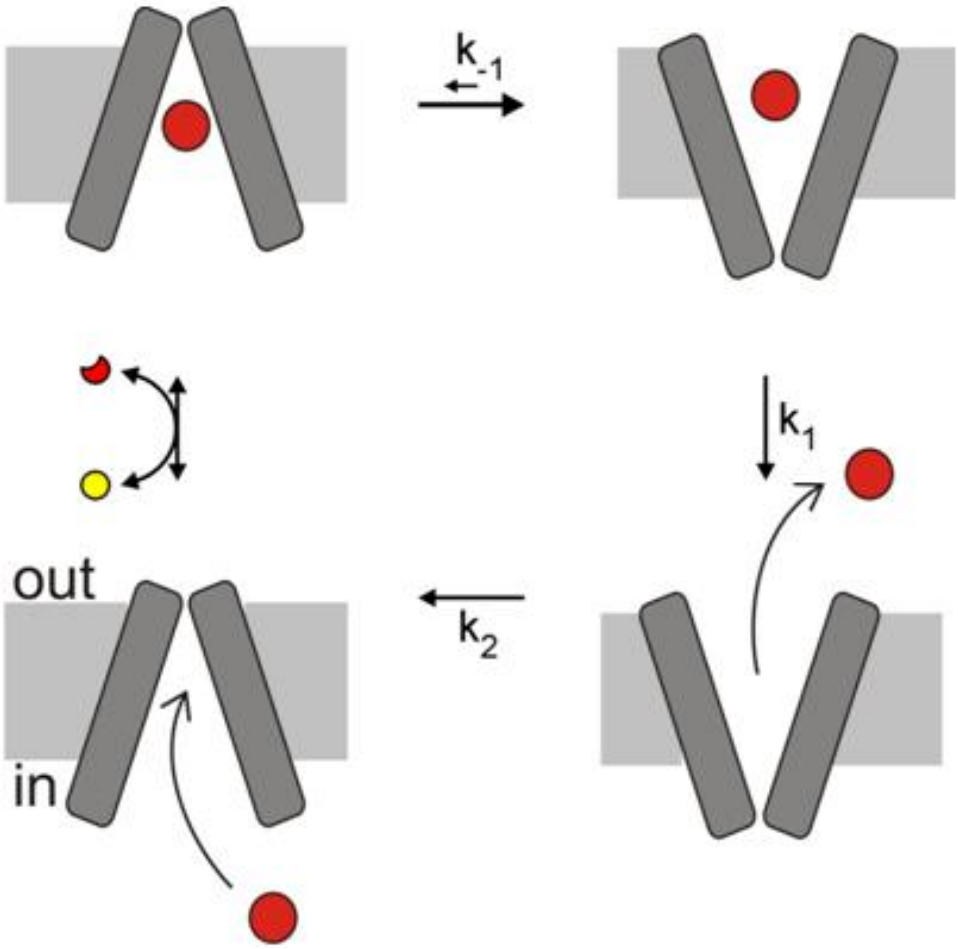

Figure 6. ABC exporter transport cycle

Cartoon representation of the functional cycle of an active transporter, mediating unidirectional, thermodynamically uphill export. The energy of ATP hydrolysis is harnessed to drive a cycle in which the TMDs alternate between inward-facing (left states) and outward-facing (right states) TMD conformations, accompanied by an affinity switch to allow high-affinity binding of the substrate in a low-concentration compartment (lower left state) and low-affinity release of the substrate in a high-concentration compartment (upper right state). Transporter TMDs, gray rectangles; ATP, small yellow circle; ADP, red crescent; substrate, large red circle.

1.4. CFTR channel gating

Although not a transporter, opening and closing (gating) of the CFTR chloride ion pore, formed by its TMDs, is coupled to the same conserved ATP binding/hydrolysis cycle at the NBDs that drives transport cycles of related ABC exporters (*Figure 7.*). As an ABC-C subfamily member, CFTR is an asymmetrical ABC protein: only the composite binding site formed by Walker A and B motifs of NBD2 and the signature sequence of NBD1 (hereafter referred to as "site 2"; *Figure 5.B, top site*) is catalytically active; the other interfacial binding site (hereafter called "*site 1*"*; Figure 5.B, bottom site*) contains several non-canonical substitutions in its key motifs, and keeps ATP bound and unhydrolyzed throughout several NBD dimerization cycles[44, 45]. In CFTR NBD dimer formation initiates a burst of pore openings interrupted by brief closures, while dimer dissociation terminates the burst and returns the TMDs into a longlasting nonconducting (interburst) state[20]. Thus, by analogy, it was suggested that in the bursting (‘‘open’’) state (*Figure 7.; right states;* O_1, O_2) CFTR’s TMDs resemble the outward-facing (cf., *Figure 6.; right states*), whereas in the interburst (‘‘closed’’) state (*Figure 7.; left states;* C_1, C_2) they resemble the inward-facing conformation of ABC exporter TMDs (cf., *Figure 6.; left states*). Indeed, functional studies have largely confirmed that assignment[46-48]. For wild-type (WT) CFTR gating is a unidirectional cycle: most openings are terminated by ATP hydrolysis (*Figure 7.; step* $O_1 \rightarrow O_2$*; rate* k_1) rather than by the far slower pathway that involves separation of the ATP-bound stable NBD dimer without hydrolysis (*Figure 7.; step* $O_1 \rightarrow C_1$*; rate* k_{-1})[49]. The mechanism of brief flickery closures ("intraburst gating") is unknown, but represents a process independent of the slow gating transitions that are coupled to NBD movements[50].

DOI:10.14753/SE.2017.2028

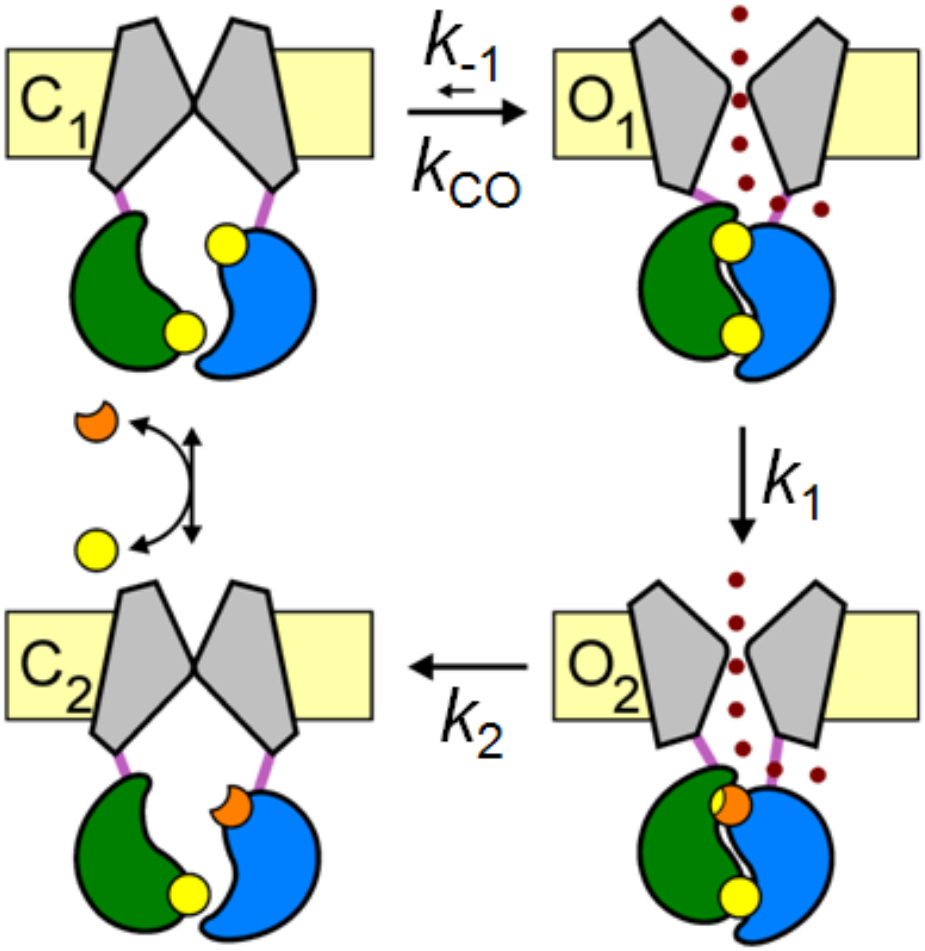

Figure 7. Wild type CFTR gating

Cartoon representation of the wild-type CFTR gating cycle. Disengaged NBDs are coupled to a closed (left states), tightly dimerized NBDs to an open pore (right states). Thus, the pore opens when the tight NBD dimer forms, and closes when the dimer interface separates – at least around site 2. However, because pore closure in the absence of hydrolysis (step $O_1 \rightarrow C_1$) is extremely slow, gating of WT CFTR is an essentially unidirectional cycle: channels open to a prehydrolytic open state (step $C_1 \rightarrow O_1$), shuttle to a posthydrolytic open state (step $O_1 \rightarrow O_2$), and then close through a pathway distinct from pore opening (step $O_2 \rightarrow C_2$). Color coding follows that of Figure 2., the R domain is not depicted. ATP, yellow circles, ADP, red crescent.

DOI:10.14753/SE.2017.2028

1.5. Studying transition-state structures

Transition states ($T^{‡}$), which determine the rates of functionally relevant conformational movements, are the highest-energy, shortest-lived conformations of proteins. For instance, for ion channels: closed → open, and open → closed conformational transitions, are so fast that they appear as single steps even in the highest time-resolution recordings. This implies that the time the channel protein spends in the $T^{‡}$ itself is on the sub-microsecond scale—in contrast to the long (milliseconds-seconds) intervals spent in comparatively stable open and closed ground states observable in single-channel recordings. Intractable by standard structural biological approaches, $T^{‡}$ structures can be studied using Rate-Equilibrium Free Energy Relationship (REFER) analysis, which reports on the relative timing of movements in selected protein regions during a conformational transition, such as a channel opening step[51, 52]. Structural perturbations (typically point mutations) in a given channel region often change channel open probability (P_o) by affecting the open-closed free-energy difference (*Figure 8.*), but the extent to which the free energy of the barrier that must be traversed in opening or closing the channel is affected, depends on how early or late that region moves.

DOI:10.14753/SE.2017.2028

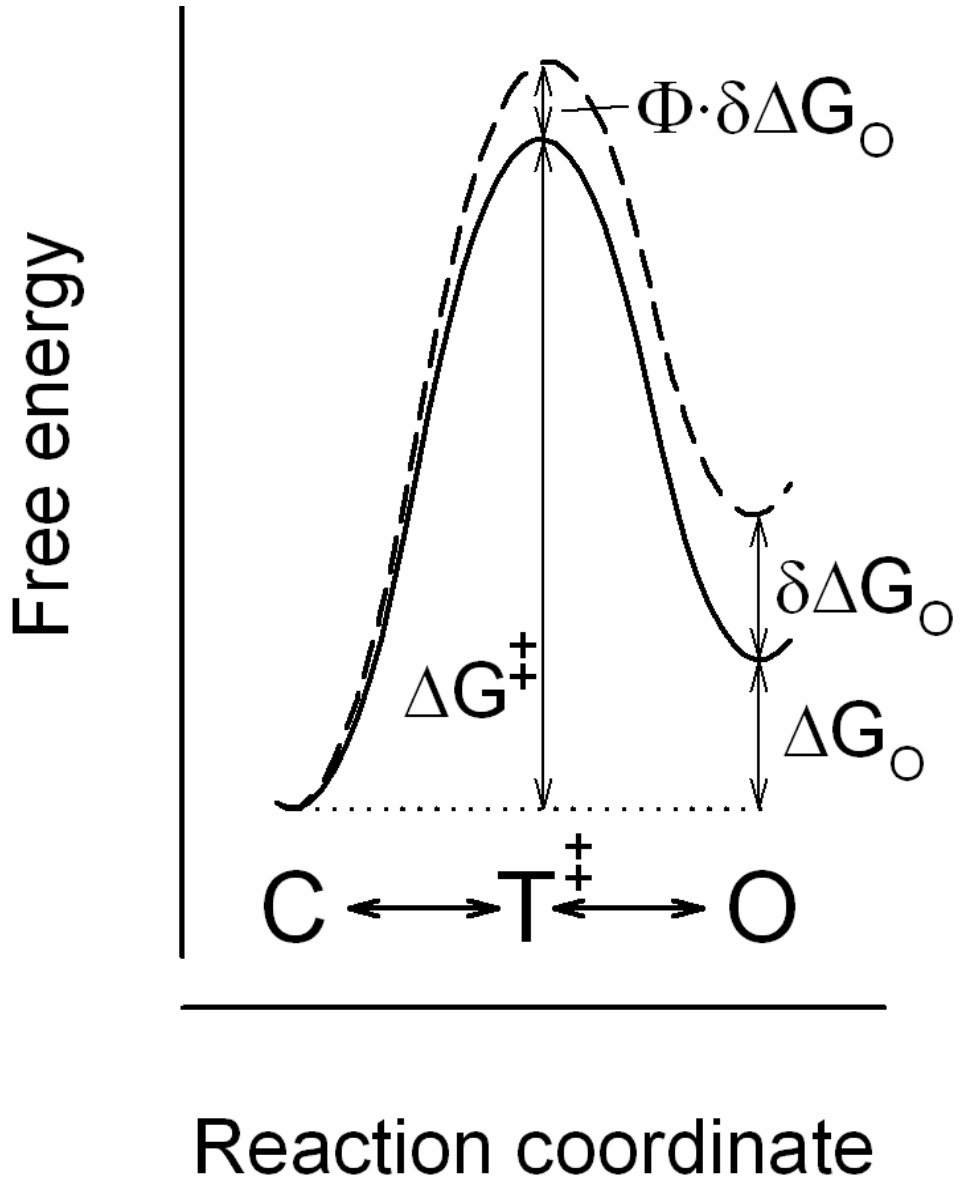

Figure 8. Effect of a perturbation on the free-energy landscape of an equilibrium reaction

The free-energy landscape for the reversible, equilibrium transition C↔T‡↔O (cf., Scheme 1 in Figure 9.) is shown without (solid line) and after (dashed line) a structural perturbation. C, O, closed and open ground states; T‡, transition state. The perturbation changes the free energy of state O by $\delta\Delta G_o$*, that of state T‡ by* $\Phi\delta\Delta G_o$ *(relative to state C). Reprinted with permission from[55].*

1.5.1. REFER theory

REFER analysis is a thermodynamic approach which provides information on transition state structures of equilibrium reactions (*Figure 9., Scheme 1)*[53, 54], but is not applicable to non-equilibrium reactions (*Figure 9.,Scheme 2*)[55]. By transition state theory, a rate k is obtained as:

$$k = A \cdot e^{-\frac{\Delta G^{\ddagger}}{RT}}$$

Equation 1.

where $\Delta G^{\ddagger}$ is the height of the free energy barrier to reach the $T^{\ddagger}$ (*Figure 8.*); R is the gas constant (8.314 J / (mol·°K)), T is the temperature in Kelvin (°K), and the prefactor A was given by Eyring in the form of k_BT/h, where k_B is Boltzmann's constant and h is Planck's constant ($k_BT/h \approx 6 \times 10^{12}$ s^{-1} at 25°C)[56]. On the assumption that the energetic perturbation of the $T^{\ddagger}$ is a linear combination of those of the ground states (*Figure 8.*)[53, 54], a structural perturbation which changes the free energy of the open ground state (relative to the closed ground state) by $\delta\Delta G_O$, will change the free energy of the $T^{\ddagger}$ by $\Phi\delta\Delta G_O$ (*Figure 8., dashed lines*), where $0 \leq \Phi \leq 1$. Thus, the logarithm of the forward rate constant (k_{CO}, *Figure 9., Scheme 1*) will change by $-\Phi\delta\Delta G_o/(RT)$:

$$\delta\left(\ln k_{CO}\right) = -\frac{\Phi\delta\Delta G_O}{RT}$$

Equation 2.

On the other hand, the equilibrium constant (K_{eq}), estimated as the probability the channel is in the open state (P_o) divided by the probability it is in the closed state ($P_c = 1-P_o$), is given by

$$\frac{P_o}{P_c} = K_{eq} = e^{-\frac{\delta\Delta G_O}{RT}}$$

Equation 3.

DOI:10.14753/SE.2017.2028

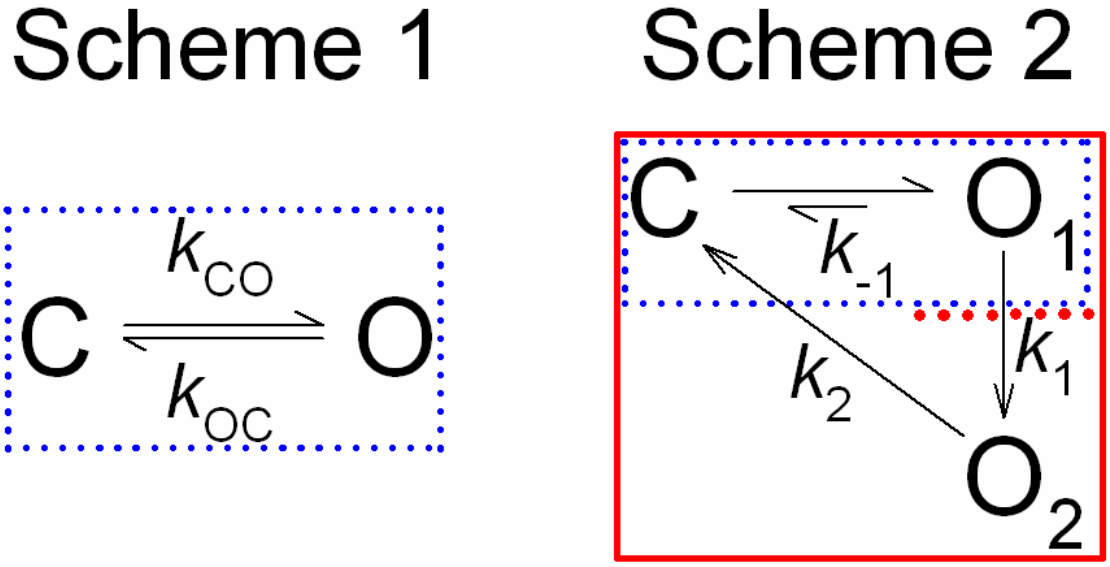

Figure 9. Equilibrium and Nonequilibrium schemes

Scheme 1, Simple equilibrium gating scheme with opening (k_{CO}) and closing rate (k_{OC}) reflecting forward and backward passage across the same free energy barrier. Scheme 2, Simplified nonequilibrium scheme of CFTR gating: the closed states in Figure 7. have been merged into a single compound state C. The C↔O_1 transition reflects formation / nonhydrolytic disruption (rate k_{-1}) of the NBD dimer; step O_1→O_2 reflects ATP hydrolysis at site 2 (rate k_1); step O_2→C represents pore closure (rate k_2). Scheme 1 can be considered a subset (dotted blue frame) of the larger Scheme 2 (red frame). Blocking the O_1→O_2 step (dotted red line) reduces Scheme 2 into Scheme 1.

DOI:10.14753/SE.2017.2028

Therefore, as a consequence of the same perturbation the logarithm of K_{eq}, will change by $-\delta\Delta G_o/(RT)$ (*Equation 4.*).

$$\delta\left(\ln K_{eq}\right) = -\frac{\delta\Delta G_O}{RT}$$

Equation 4.

A REFER plot is a log-log plot of k_{co} versus K_{eq}, for a series of structural perturbations introduced into a single region of a protein (*Figure 10.*). Because the ratio Φ between the effects on transition-state and open-state stabilities is similar for perturbations of a single protein position, the slope of this plot reports the value of Φ, as can be easily seen by dividing *Equation 2* by *Equation 4*:

$$\Phi = -\frac{\delta\left(\ln k_{CO}\right)}{\delta\left(\ln K_{eq}\right)}$$

Equation 5.

DOI:10.14753/SE.2017.2028

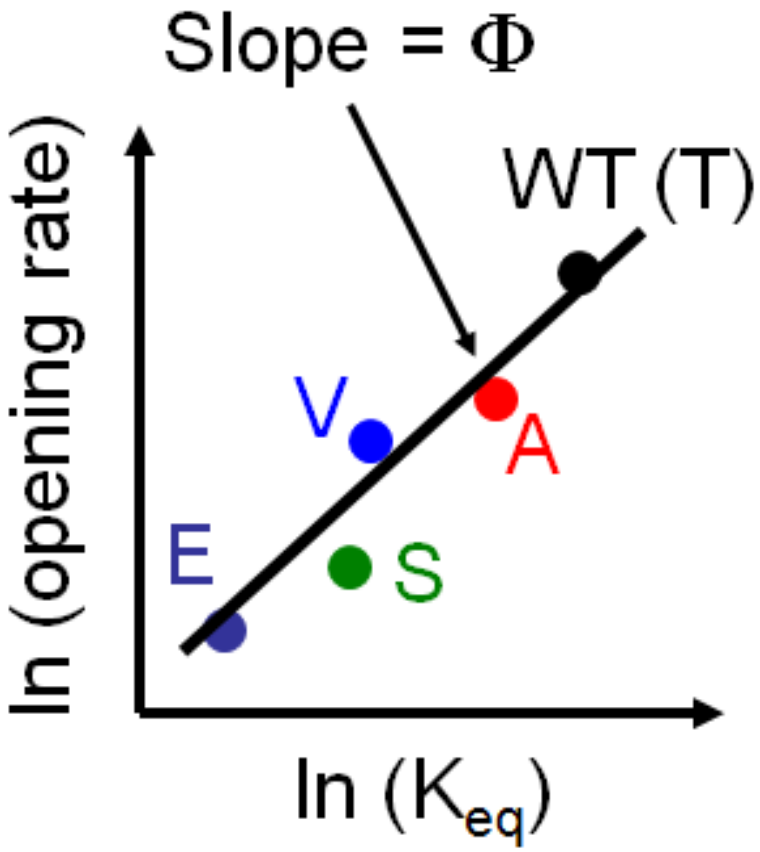

Figure 10. Construction of a Brønsted plot

A Brønsted plot is a plot of $\ln k_{co}$ *vs.* $\ln K_{eq}$ *for a number of mutations at a particular site of the protein. Both the open-closed equilibrium constant* ($K_{eq}=P_o/(1-P_o)$)*, and the opening rate* (k_{CO}) *can be determined in single-channel recordings. Thus, on a Brønsted plot the WT channel is represented by a dot (black dot). Introducing a series of different substitutions into a certain protein position (in the illustration the WT channel contains a threonine in the target position which is substituted for a glutamate, serine, valine, or alanine), each substitution alters the open-state and transition-state stabilities to different extents: thus, each mutant is represented by a distinct spot in the plot (colored spots). Because the ratios between the effects on transition-state and open-state stabilities are similar for perturbations of a single protein position, these spots fall onto a straight line, the slope of which provides an estimate for the* Φ *value of that protein region.*

1.5.2. Interpretation of the Φ-value

A region that moves early during opening will have already approached its open-state conformation in the overall transition state: a perturbation here thus affects the stability of the transition state to an extent similar to that of the open state (Φ=1). Thus, the height of the barrier for the opening transition changes, but the height of the barrier for the closing transition does not, so a perturbation in such a region impacts only opening, but not closing, rate (*Figure 11.A*). In contrast, a region that moves late during opening is still near its closed state conformation in the transition state, thus, perturbations here that affect open-state stability do not affect transition state stability. As a consequence, the height of the barrier for the closing transition changes, but the height of the barrier for the opening transition does not, so perturbations in such a region impact only closing, but not opening, rate (*Figure 11.C*). Finally, a region which is just on the move in the transition state, i.e., is in an intermediate conformation between its closed-like and open-like conformations, will be characterized by an intermediate Φ value: by affecting the height of the barrier both for the opening and the closing transition, perturbations in such a region impact both opening rate, and closing rate, but in opposite directions (*Figure 11.B*). In reality, energy landscapes for ion-channel gating transitions are more complex, but experimental Φ values still reflect the temporal sequence in which different regions of the protein move[51].

1.6. A CFTR construct suitable for REFER analysis

REFER analysis has been extremely fruitful in mapping gating dynamics of the nicotinic acetylcholine receptor channel[57-60] but is applicable only to equilibrium mechanisms[55], unlike that of WT CFTR. This drawback has so far hampered insight into the CFTR opening transition state. Although two REFER studies on CFTR have been published in the past[61, 62], it has been demonstrated[55] that this methodology can provide no useful information on the non-equilibrium cyclic mechanism (*Scheme 2*, *Figure 9.*) which governs WT CFTR bursting[49]. In addition, applying REFER analysis to the equilibrium transition to and from flickery closures[62] (transitions that have a negligible effect on P_o[50]) has limited relevance to CFTR function.

DOI:10.14753/SE.2017.2028

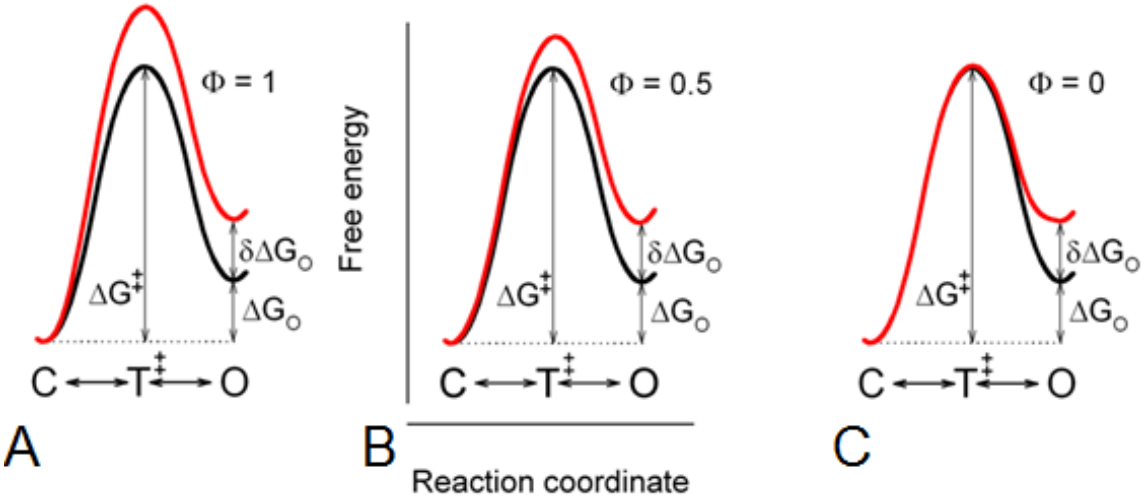

Figure 11. Effects on the free energy landscape of perturbations in a protein region depend on the relative timing of its movements.

All three graphs illustrate the free-energy landscape for the reversible, equilibrium transition $C \leftrightarrow T^{\ddagger} \leftrightarrow O$ without (black lines) and after (red lines) a structural perturbation.(notations follow that in Figure 8.). A, a region that moves early during opening will have already approached its open-state conformation in the overall $T^{\ddagger}$: perturbations here affect the stability of the transition state to an extent similar to that of the open state. B, Perturbations of a region that is just on the move in the $T^{\ddagger}$ affect transition state stability to a smaller extent than open-state stability. C, A region that moves late during opening is still near its closed state conformation in the $T^{\ddagger}$: a perturbation here that affects open-state stability does not affect transition state stability.

To appropriately adapt the REFER technique to CFTR gating, a suitable construct is required, the gating of which approximates a simple equilibrium closed-open scheme (*Scheme 1, Figure 9.*).

Hydrolysis-disrupting mutations (*Figure 12., red star*) truncate the normal CFTR gating cycle by blocking the ATP hydrolysis step $O_1 \rightarrow O_2$ (*Figure 9., dotted red line in Scheme 2; Figure 12., red cross*), thereby reducing it to an equilibrium reaction (*Scheme 1 in Figure 9.*). Among many known hydrolysis-deficient CFTR mutants D1370N appeared as an attractive choice for a REFER study, because its unusually fast non-hydrolytic closing rate (~0.5 s^{-1}) allows single-channel gating analysis[49, 50], while ATP-dependence of channel opening was shown to be little changed[50]. When studied in the presence of saturating ATP, the gating mechanism of such channels approximates a simple two-state scheme: reversible transitions between states C_1 and O_1 (*red box in Figure 12.*).

A second problem which must be addressed for proper interpretation of REFER data is potentially altered phosphorylation-dependent regulation of mutant channels (e.g.,[63]). Indeed, recent evidence suggests that the R domain regulates CFTR gating by directly interacting with the TMDs[64, 65]. To selectively study the energetics of ATP-dependent gating, confounding effects of potentially altered TMD-R domain interactions must therefore be eliminated by using a CFTR construct lacking the R domain (ΔR). The modular ABC architecture offers a natural strategy to achieve that goal: functional CFTR channels can be obtained by the coexpressing NBD1-TMD1 (residues 1-633) and NBD2-TMD2 (residues 837-1480) as separate polypeptides – a strategy nature employs for most prokaryotic ABC proteins. This "cut-ΔR" CFTR was shown to be active without prior phosphorylation but indistinguishable from (prephosphorylated) WT CFTR with respect to ATP-dependent gating[49]. This minimalist channel – pared down to the essential ABC domains and containing the D1370N mutation in the NBD2 head (*Figure 13.*) – therefore appeared as an attractive candidate background for a REFER study aimed at obtaining meaningful biophysical information on CFTR channel opening dynamics.

DOI:10.14753/SE.2017.2028

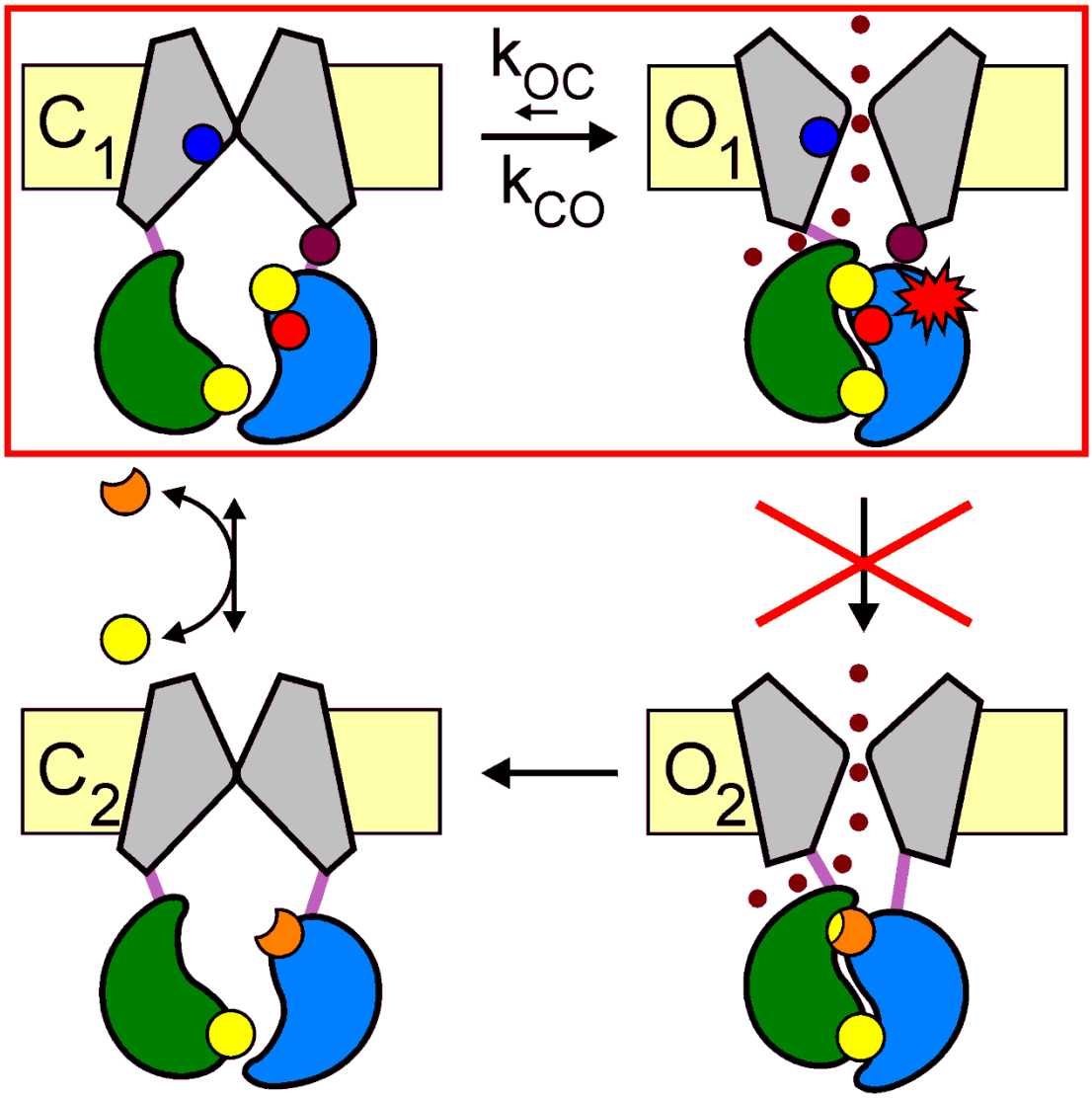

Figure 12. Reducing CFTR gating to a two-state scheme by abrogating ATP hydrolysis

Cartoon representation of the CFTR gating cycle replotted from Figure 7. The D1370N mutation (red star in NBD2 head) abrogates ATP hydrolysis (red cross) and confines gating in saturating ATP to the simple equilibrium two-state closed-open scheme $C_1 \leftrightarrow O_1$ *(red box). Positions targeted for REFER analysis are depicted as small colored circles: 1246 (red), 275 (light violet), 348 (dark blue).*

DOI:10.14753/SE.2017.2028

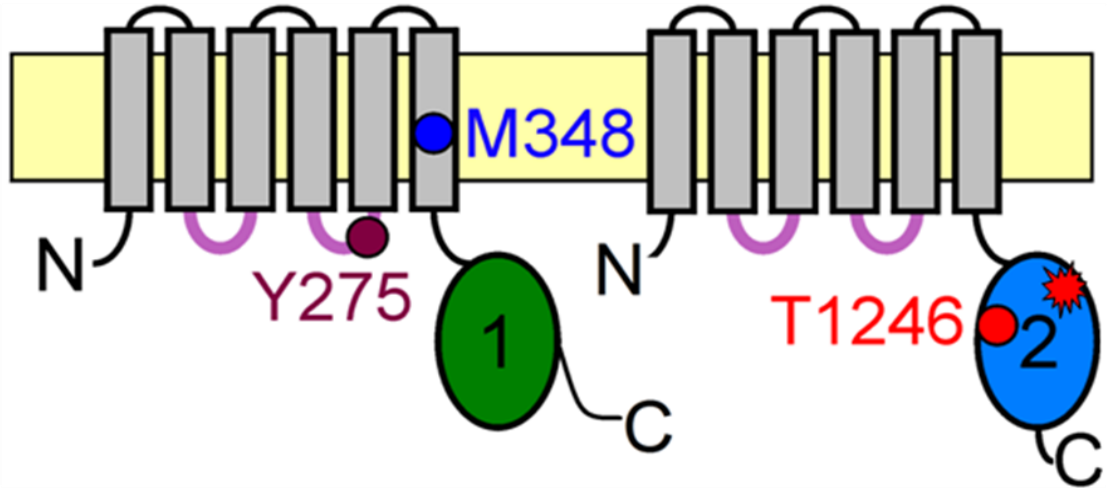

Figure 13. Domain topology of REFER background construct, and positions of amino acids selected for point mutagenesis.

Left half-construct: TMD1-NBD1 (residues 1-633). Right half-construct: TMD2-NBD2 (residues 837-1480) containing mutation D1370N (red star in NBD2). Purified cRNA for both half constructs is co-injected into Xenopus laevis oocytes, and translated into separate polypeptides. Positions targeted for REFER analysis (small colored circles: 1246 (red), 275 (light violet), 348 (dark blue)) are mapped to reflect their approximate positions in the primary sequence.

DOI:10.14753/SE.2017.2028

1.7. Therapeutic relevance of mechanistic studies

A large fraction of CF mutations, including those which impair protein folding/trafficking (e.g. ΔF508, constituting >70% of CF alleles) are associated with severe gating defects. The ΔF508 mutation reduces opening rate, k_{CO}, approximately 25-fold[66], reporting a substantial mutation-induced destabilization of the opening transition state. Thus, in addition to mending the folding defect, efficient pharmacological treatment of CF will need to employ strategies that improve gating. On the other hand, in secretory diarrheas efforts to reduce CFTR channel activity in intestinal epithelial cells could moderate the excessive apical Cl^-, and hence water flux. Based on CFTR's unique cyclic mechanism a novel intervention strategy for altering channel P_o has recently been suggested: for a strictly cycling mechanism large effects on P_o can be achieved by affecting transition-state energetics – in contrast to equilibrium mechanisms for which such maneuvers alter transition rates but not P_o[67]. For instance, a stabilization of the $C_1 \leftrightarrow O_1$ transition state by just 1 kT (assuming rates $k_{co}=1s^{-1}$, $k_{-1}=0.2s^{-1}$, $k_1=5s^{-1}$ in *Figure 7.*; typical for WT CFTR in saturating ATP), predicts an increase in P_o from 0.17 to 0.35. This is because a simultaneous *e*-fold increase in rates k_{co} and k_{-1} increases opening rate by *e*-fold, while strict cycling, and thus closing rate, are little affected.

Thus, insight into the dynamics of the opening conformational change and the structure of its transition state would be beneficial in two ways. First, it would constitute a key step forward in understanding the molecular mechanism of the ΔF508 gating defect. Second, it would promote the design of drugs that enhance P_o by improving transition-state stability.

DOI:10.14753/SE.2017.2028

2. Objectives

2.1. To choose an appropriate background construct suitable for REFER studies

Our first goal was to establish a background construct suitable for studying the CFTR opening conformation change using the REFER approach. Essential criteria for such a construct are that (i) its gating should be at equilibrium, (ii) its affinity for ATP – even in the presence of all tested target-site mutations – should remain high enough to allow experiments to be conducted under saturating conditions, (iv) perturbation-induced changes in gating kinetics should reflect changes in ATP-dependent, rather than phosphorylation-dependent mechanisms, and (iv) its gating transitions should be fast enough to afford collection of sufficient numbers of gating events for reliable kinetic analysis.

2.2. To study the global conformational wave along the longitudinal protein axis

With a suitable experimental system at hand we would like to get information on how conformational changes are propagated along the longitudinal axis (cytoplasmic to extracellular) of the molecule. To this end, we will aim to compare the relative timing of opening-associated conformational movements in three spatially distant protein regions: (i) composite site 2 of the NBD1-NBD2 interface, (ii) the NBD2-TMD interface, and (iii) the pore region. For the latter region we hope to employ two types of perturbations: point mutagenesis and anion substitution.

3. Methods

3.1. Molecular biology

All constructs were made starting from pGEMHE-CFTR(837-1480) (N-half) and pGEMHE-CFTR(1-633) (C-half)[69]. First, mutation D1370N was introduced into C-half to generate C-half(D1370N). Mutations of target positions 275 and 348 were introduced into N-half, and those of target position 1246 into C-half(D1370N). All mutagenesis was done using the Stratagene QuickChange Kit, and all constructs were verified by automated sequencing. cDNA was transcribed in vitro using T7 polymerase (Ambion mMessage Kit), and then run on denaturing gels to check size and quality. RNA concentration was estimated by comparison with known amount of 0.24-9.5 kb RNA ladder (GIBCO).

3.2.Heterologous expression: Isolation and injection of *Xenopus laevis* oocytes

Stage V-VI oocytes were isolated from adult female *Xenopus laevis* by partial ovariectomy under ethyl 3-aminobenzoate methanesulfonate salt (4g/400mL solution) anesthesia, and were defolliculated by one-to-two hour treatment, at 18^{o}C, with 20 mg/mL collagenase (gibco; type II type) in Ca^{2+}-free oocyte Ringer's solution (*OR2, Table 1., row 1*). Defolliculated oocytes were rinsed extensively with Ca^{2+}-free OR2 (3-5 washes, 50 mL each), and then incubated at 18^{o}C for several hours in OR2 supplemented with 1.8 mM Ca^{2+} and 1 mM gentamycin (*OR2+, Table 1., row 2*), before they were pressure-injected (Nanojet, Drummond) with cRNA. Injection pipettes were pulled with a micropipette puller (Narishige, PP-83) from glass capillaries (# 3-000-203-G/X, Drummond) and their tips were broken to an internal diameter of 10-20 μm. Usually, and unless otherwise specified, 0.1-10 ng of each half-construct cRNA, premixed for coexpression, in a constant volume of 50 nL, were injected per oocyte; the amounts of injected cRNA were chosen depending on the expression level needed. Injected oocytes were further incubated at 18^{o}C for a period of 6 hours to 5 days before they were used for recording.

3.3. Excised patch recording

For recording single-channel or macroscopic currents, excised inside-out patches were pulled from pre-injected oocytes. Oocytes were shrunk for approximately 1 minute in a hypertonic pealing solution (*PLS1, Table 1., row 3*), the vitelline membranes removed manually, and the cells transferred to a recording chamber containing standard bath solution (*BS3-Cl, Table 1., row 4*).

Patch pipettes were pulled from borosilicate glass (Drummond, cat.#N-51A) using a vertical pipette puller (Narishige, PP-83). Tips were heat-polished to a diameter of 1-2 μm (4-7 MΩ), or 5-6 μm (~1 MΩ), for single-channel or macropatch recordings, respectively. Pipettes were back-filled with pipette solution (*PS3, Table 1. final row*) using a micro-syringe. Seals in the 100-300 GΩ range were routinely obtained.

Patches were excised and transferred to a flow chamber, where the cytoplasmic surface was continuously superfused with standard bath solution containing various test substances. Switching between solutions was implemented by computer-driven electric valves (Scientific Instruments, VC83 valve commander). With a dead volume of approximately 20 μL and a flow rate of around 0.5 mL/min, complete solution exchange took 2-4 seconds. The kinetics of solution exchange was characterized by a delay of ~1 second, followed by a transition period with a time constant of ~100 ms; as verified at the end of each recording by applying a brief pulse of 2 mM Ca^{2+}, and observing the rate of decay of endogenous Ca^{2+}-activated Cl^--channel current upon Ca^{2+} removal.

In the case of chloride-based bath solutions the bath electrode (Ag/AgCl pellet) was immersed directly into the flow chamber. In experiments that involved replacement of the bath anion the electrode was placed in 100mM KCl and connected to the flow chamber by an agar bridge (4% agar in 100mM KCl). CFTR channels were activated by 10 mM Magnesium-ATP added, from a 400-mM aqueous stock solution (pH = 7.1 with NMDG), into a specified bath solution (Table 1., rows 5-8). Recordings were done at ambient room temperature which varied between 23-26 ^oC. The holding potential was at -80 mV (-100 mV for formate currents), and currents were recorded (EPC7, Heka Elektronik amplifier) at a bandwidth of 2 kHz and digitized at 10 kHz. Single-channel patches were identified as very long (typically 15 min–1 hr) recordings without superimposed channel openings.

DOI:10.14753/SE.2017.2028

Table 1. Experimental solutions

Solution long name	**Solution short name**	**Composition**	**pH**
oocyte Ringer's solution #2	OR2	82.5 mM NaCl, 2 mM KCl, 1mM $MgCl_2$, 5 mM HEPES	7.5
oocyte Ringer's solution #2+	OR2+	82.5 mM NaCl, 2 mM KCl, 1mM $MgCl_2$, 5 mM HEPES, 1.8 mM $CaCl_2$, 1 mM gentamycin-sulfate	7.5
Pealing solution #1	PLS1	138 mM NMG, 2 mM $MgCl_2$, 5 mM HEPES, 0.5 mM EGTA, 134 mM HCl ,100 mM NaCl	7.1
Bath solution #3 chloride	BS3-Cl	138 mM NMG, 2 mM $MgCl_2$, 5 mM HEPES, 0.5 mM EGTA, 134 mM HCl	7.1
Bath solution #3 formate	BS3-Fm	138 mM NMG, 2 mM $Mg(OH)_2$, 5 mM HEPES, 0.5 mM EGTA, 138 mM Formic acid	7.1
Bath solution #3 bromide	BS3-Br	138 mM NMG, 2 mM $Mg(OH)_2$, 5 mM HEPES, 0.5 mM EGTA, 138 mM HBr	7.1
Bath solution #3 nitrate	BS3-Ni	138 mM NMG, 2 mM $Mg(OH)_2$, 5 mM HEPES, 0.5 mM EGTA, 138 mM nitric acid	7.1
Pipette solution #3	PS3	138 mM NMG, 2 mM $MgCl_2$, 5 mM HEPES, 136 mM HCl	7.4

3.4. Idealization and burst analysis of multi-channel patches

Baseline-subtracted current traces were digitally filtered at 20Hz (10 Hz for anion substitution experiments), and idealized using a simple half-amplitude threshold crossing criterion. While the vast majority of patches included in the analysis contained only 1 active channel, in a few cases that allowed reliable estimation of channel number events lists from records with 2 or 3 active channels were also included. Events lists from such recordings were fitted with a model in which ATP-dependent gating transitions were pooled into a closed-open scheme, and the flickery closures modeled as pore blockage events[68], resulting in the three-state closed-open-blocked) scheme (C-O-B). The best set of rate constants r_{CO}, r_{OC}, $r_{OB,}$ and r_{BO} was extracted[69] from a simultaneous maximum likelihood fit to the dwell-time histograms, which accounts for the filter dead time (9 ms). Mean interburst (τ_{ib}) and burst (τ_b) durations were then calculated as $\tau_{ib}=1/r_{CO}$, and $\tau_b=(1/r_{OC})(1+ r_{OB}/r_{BO})$.

3.5. Burst analysis of single-channel patches

Bursts were isolated from single-channel records by suppressing closures shorter than a specified cutoff (t_c). The method of Magleby and Pallotta (1983) was used to choose the value of t_c individually for each record; this method ensures unbiased estimation of τ_b and τ_{ib} durations by equalizing the probabilities of misassigning interburst events as flickery closures and vice versa. The arithmetic averages of the durations of the bursts and interbursts obtained this way were taken as individual estimates of τ_b and τ_{ib} in a particular patch, and statistics was done on data from several patches. All data are given as mean ± SEM of measurements from at least 4 (typically 5–8) long segments of single-channel recordings, from 4–13 patches for each mutant; in the face of alternating periods of lower and higher activity typical to CFTR[70], several hours of total recording for each construct were obtained to ensure unbiased sampling of average gating behavior.

3.6. Calculation of apparent affinities for ATP and fitting macroscopic current relaxations upon ATP removal

For constructs that afforded macroscopic currents closing rates were also verified from exponential fits to macroscopic current relaxations upon ATP removal.

Because of the relatively lower expression of all of our constructs, compared to WT CFTR, we could obtain macroscopic currents from tens to hundreds, but not hundreds to thousands, of channels in an inside-out patch. However, time courses of such currents were still adequate for reliable fitting. The macroscopic currents were digitally re-filtered at 10Hz using a Gaussian filter, and then sampled at 50 Hz. Decay currents following sudden ATP removal were fitted by single exponentials using a least-squares fitter (SigmaPlot), and the relaxation time constants (τ_{relax}) compared with steady-state τ_b. The average steady-state current during 1-2-minute applications of test concentrations of MgATP was normalized to the mean of the steady currents in 10 mM MgATP before and after the test, and the ratios used to estimate apparent affinities for ATP.

3.7. REFER analysis

For each target site five substitutions were chosen so as to perturb structure as little as possible, but still sufficiently alter P_o for reliable Φ estimation. In general, side chains of various sizes, polarities and charges were chosen. Experiments were done at saturating [ATP] determined individually for each construct, to ensure that the channel opening step is not rate limited by ATP binding.

Mean interburst and burst durations obtained from steady-state burst-analysis of microscopic currents in 10 mM ATP (see sections 3.4. and 3.5.) were used to define opening (k_{CO}) and closing (k_{OC}) rates as $1/\tau_{ib}$ and $1/\tau_b$, respectively; K_{eq} was then defined as k_{CO}/k_{OC}. Brønsted plots (ln k_{CO} vs. ln K_{eq}) were fitted by linear regression.

DOI:10.14753/SE.2017.2028

4. Results

4.1. Choice of a background construct suitable for REFER studies

ATP hydrolysis in ABC proteins is destroyed by mutations of the Walker B aspartate[71-73], that coordinates Mg^{2+} at each active site[11, 16]. To induce equilibrium gating in CFTR, we introduced the NBD2 Walker-B mutation D1370N (*Figure 12. and 13., red star*). Amid several hydrolysis-disrupting mutations tested, D1370N only slightly reduces the apparent affinity for ATP, and does not prolong open bursts to an extent incompatible with single-channel gating analysis[49]. For example, mutations of the NBD2 Walker A lysine (K1250) or proposed catalytic carboxylate (E1371), shown to abolish or severely impair ATP hydrolysis in CFTR and other ABC proteins[20], prolong τ_b by several orders of magnitude[20] (*Figure 14.*), making collection of sufficient numbers of single-channel gating events a daunting task. In contrast, τ_b is prolonged only by ~10-fold in D1370N, likely due to a somewhat reduced NBD dimer stability.

PKA- and ATP-dependent regulation of CFTR gating are intertwined, and the mechanism of R-domain action is poorly understood: evidence exists for its direct interaction with both NBDs and TMDs[74, 75]. Thus, changes in gating kinetics caused by perturbations of a target position might potentially reflect altered R-domain/target position interactions, rather than energetic effects on ATP-dependent conformational transitions. Such confounding effects are absent in channels lacking the R domain: cut-ΔR channels, obtained by coexpression of TMD1-NBD1 (residues 1–633) and TMD2-NBD2 (residues 837–1480), do not require phosphorylation to be active, while ATP-dependent gating remains similar to WT[69]. Thus, we chose cut-ΔR(D1370N) as the background construct for our REFER study (*Figure 13.*), and started off by its thorough functional characterization.

DOI:10.14753/SE.2017.2028

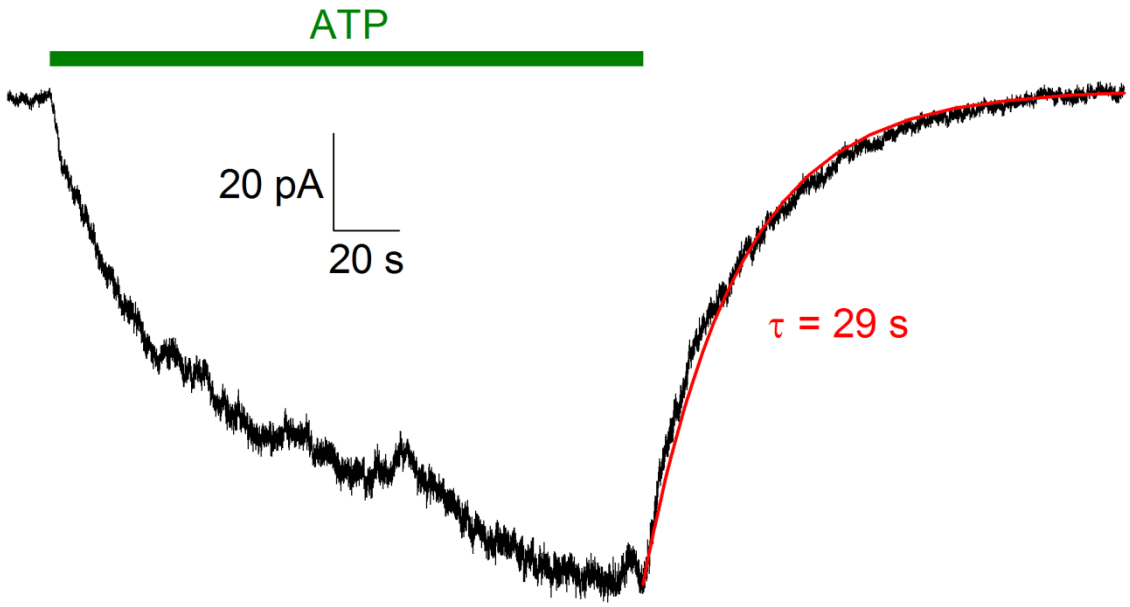

Figure 14. Excessively long bursts of K1250A CFTR preclude single-channel gating analysis

Macroscopic current of prephosphorylated K1250A CFTR channels was activated by application of 10 mM ATP. Time course of current decay upon ATP removal was fitted by a single exponential (red line), the time constant (τ) reflects mean burst duration.

Gating of cut-ΔR(D1370N) indeed proved PKA-independent but remained strictly ATP-dependent with an apparent affinity for ATP of 288 ± 27 μM (*Figure 15.A-B*). Just as for WT[50, 69, 76, 77], cut-ΔR[69, 70], and D1370N[50] CFTR channels, τ_b of cut-ΔR(D1370N) proved largely ATP-independent: the time constant of macroscopic current relaxation following ATP removal (*Figure 16.E*), a measure of τ_b in zero ATP, was 1,342 ± 72 ms; which is similar to the steady-state τ_b of 1,526 ± 301 ms (*Figure 16.C*) for single channels opening and closing in saturating (10 mM) ATP (*example single channel recording, Figure 16.A*). Thus, ATP-dependence of P_o *(Figure 15.*) reflects ATP dependence of its τ_{ib}. Importantly, in saturating (10 mM) ATP τ_{ib} *(Figure 16.D*) is minimal, and bursting of this background construct is reduced to a simple equilibrium (*$C_1 \leftrightarrow O_1$; Figure 12., red box*) as reported by reasonable fits of the distributions of both burst- and interburst-durations by single exponentials (*Figure 17.*). These features identify cut-ΔR(D1370N) as a suitable construct for study by the REFER approach.

4.2. Tracking the global conformational wave of channel opening

4.2.1. Timing of movement in composite site 2 of the NBD1-NBD2 interface

NBD2 Walker-A threonine 1246 makes important contributions to forming composite site 2 of the CFTR NBD1-NBD2 dimer, by contacting the γ-phosphate of ATP (PDBID: 3GD7). Moreover, this interfacial residue undergoes relative movement upon NBD dimerization, as reported by interaction of its side chain across the dimer interface with that of opposing NBD1 residue R555 in open, but not in closed, channels[20]. To test timing of relative movement at this NBD interface position, we created a series of mutants by replacing the native threonine.

DOI:10.14753/SE.2017.2028

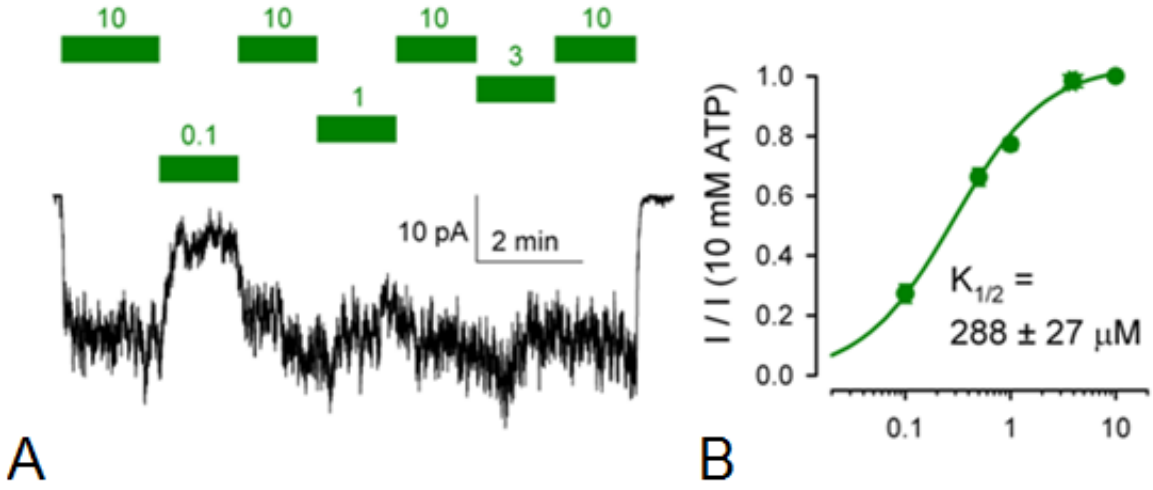

Figure 15. Macroscopic inward current and Dose response curve for cut-ΔR(D1370N) CFTR

A, Macroscopic inward cut-ΔR(D1370N) CFTR channel current in an inside-out patch recorded at -80 mV in response to exposures (green bars) to various concentrations (green numbers, in mM) of MgATP.

B, Dose response curve of fractional macroscopic currents in various test [ATP], normalized to the mean of the currents in the presence of bracketing applications of 10 mM ATP. All data are shown as mean ± SEM (n = 5-10). Solid line is a Michaelis-Menten fit through the data with $K_{1/2}$ indicated.

DOI:10.14753/SE.2017.2028

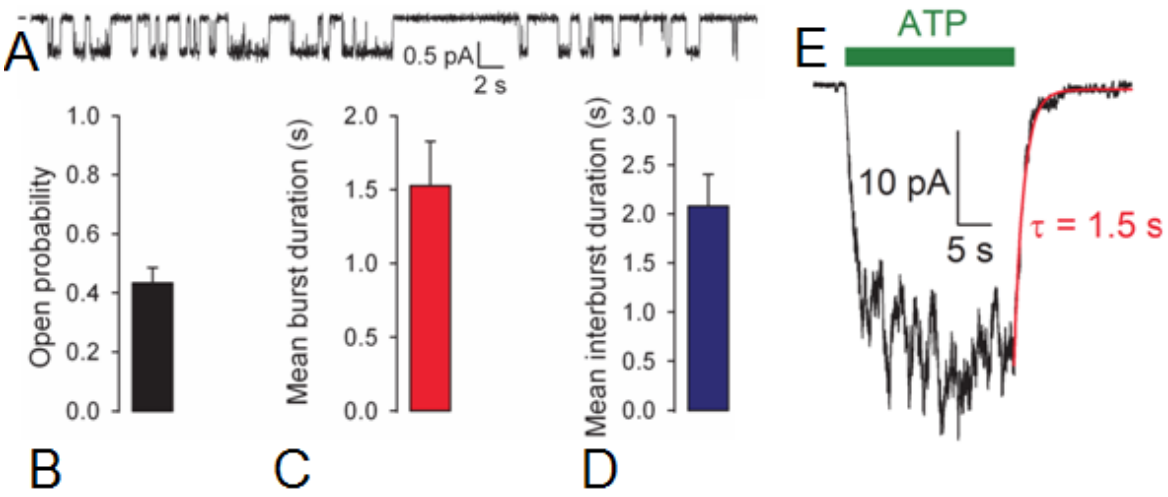

Figure 16. Gating parameters for CFTR-cut-ΔR(D1370N)

A, Background construct, sample 1 minute current trace of a single cut-ΔR(D1370N) CFTR channel opening and closing in the presence of 10 mM ATP.

Parameters for cut-ΔR(D1370N) in 10 mM ATP, obtained from steady-state single-channel recordings: B, open probability; C, mean burst duration; D, mean interburst duration.

E, Macroscopic current of cut-ΔR(D1370N) CFTR channels activated by brief 10 mM ATP exposure. Time course of current decay upon ATP removal was fitted by a single exponential (red line), the time constant (τ) reflects mean burst duration in zero ATP.

DOI:10.14753/SE.2017.2028

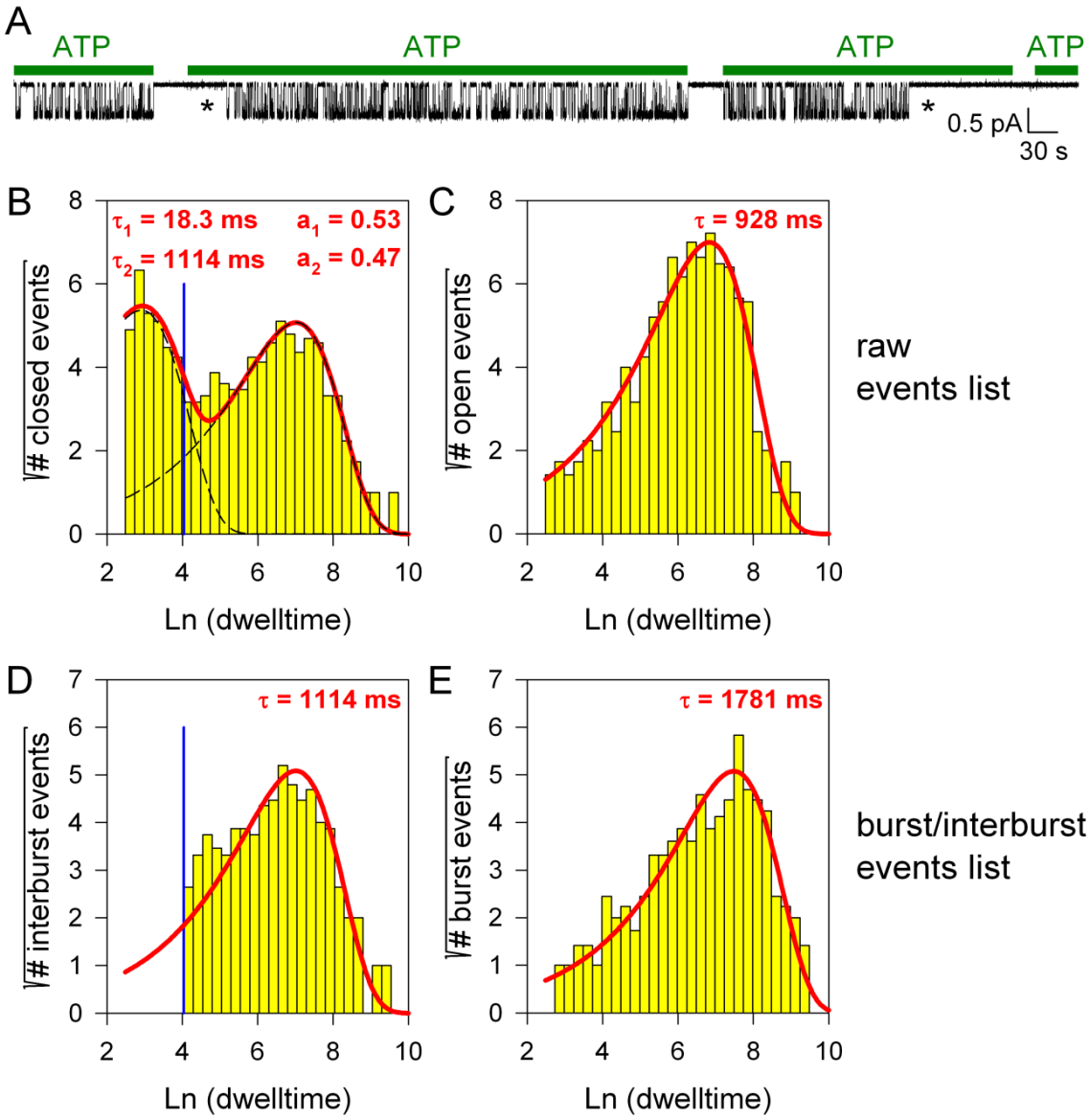

Figure 17. Burst Analysis of Cut-ΔR(D1370N) Single-Channel Recording.

Inward current of a single cut-ΔR(D1370N) channel repetitively exposed to 10 mM MgATP (green bars). Upon readmission of ATP following prolonged exposure to an ATP-free solution channels sometimes reopen with a marked delay (first asterisk); infrequently channels also inactivate in the continued presence of ATP (second asterisk). Such inactive periods were identified by eye, and excluded from our analysis. (B and C) Closed (B) and open (C) dwell-time histograms[78] constructed from the events list of the record in A; lower binning limit is 12 ms. Solid red lines are maximum likelihood fits of the dwell-times by a double- and a single-exponential distribution, respectively, with time constants ($\tau_{(1,2)}$) and fractional amplitudes (a_1, a_2) printed in the panels.

...Continuation of Figure 17.

Dotted black lines in panel B depict the two components of the fit; vertical blue line marks the burst delimiter (t_{crit}) calculated using the method of Magleby and Pallotta (1983)[79]: this method ensures unbiased estimation of mean burst and interburst durations by equalizing the probabilities of misassigning interburst events as flickery closures and vice versa. (D and E) Dwell-time histograms of reconstructed interburst (D) and burst (E) events following suppression of closed events shorter than t_{crit}. Solid red line in (D) replots the longer component of the double-exponential fit in (B): note, some flickery closures remain uncancelled (events above red fit line, right of blue line), but an equal number of interburst closures is cancelled (lack of events below red fit line, left of blue line). Solid red line in (E) is a maximum likelihood fit of the burst durations by a single-exponential distribution (τ, time constant).

DOI:10.14753/SE.2017.2028

The latter was replaced with valine, proline, cysteine, asparagine, and alanine, and the gating kinetics of each mutant was characterized in inside-out single channel patches superfused with 10 mM ATP (*Figure 18.A*).

All of these perturbations dramatically reduced P_o (*Figure 18.A and D*) by prolonging mean interburst duration (τ_{ib}; *Figure 18.A and C*), i.e., by slowing channel opening rate ($k_{CO}=1/\tau_{ib}$). In comparison, τ_b, and hence closing rates ($1/\tau_b$), were less affected (*Figure 18.A and B*). Correspondingly, the Brønsted plot for position 1246 yielded a steep slope of $\Phi=0.97\pm0.19$ (*Figure 18.E*), indicating that this position moves very early during the pore opening conformational transition. Importantly, although mutations at position 1246 slightly reduce the affinity for ATP binding[20], 10 mM ATP remained saturating for each of the mutants, as indicated by near-maximal currents already in 3 mM ATP (*Figure 19.C*) This confirms that the reduced opening rates of the T1246 mutants indeed reflect slowing of step $C_1 \rightarrow O_1$ (k_{CO}, *Figure 12.*).

The T1246A mutant expressed well enough to afford macroscopic current relaxation measurements; its macroscopic closing time constant following removal of 10 mM ATP (*Figure 19.A-B*) matched its steady-state mean burst duration, and was similar to that of the background construct (*Figure 19.B*).

Whereas estimation of τ_b does not require correct estimation of the number of active channels (*N*) in the patch, estimates of τ_{ib}, and therefore of P_o, are highly sensitive to the assumed value of *N*. Counting channels becomes exceedingly difficult when the P_o is very low, as in the case of the T1246 mutants. Therefore, efforts were made to identify, and exclude, patches in which more than a single channel contributed to the observed gating events. True single-channel patches were identified as very long (typically 15 min–1 hr) recordings without superimposed channel openings. In addition, T1246 mutants were strongly stimulated by 2'-deoxy-ATP, which was therefore applied at the end of each experiment, to facilitate detection – or exclusion – of the presence of a second active channel in the patch (*Figure 20.*).

DOI:10.14753/SE.2017.2028

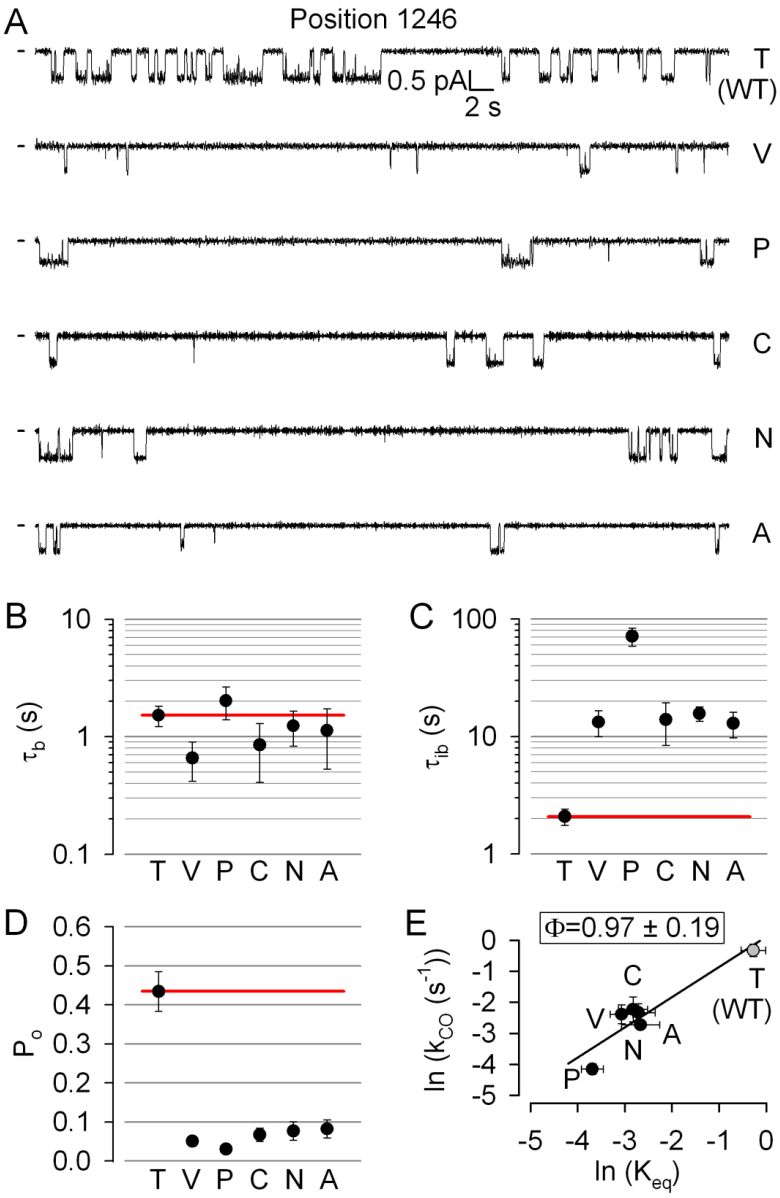

Figure 18. Timing of motion at position 1246 of the NBD1-NBD2 interface.

A, Inward single-channel currents of the cut-ΔR(D1370N) CFTR background construct (top trace), and of channels bearing mutations T1246V, T1246P, T1246C, T1246N, and T1246A, respectively, in the same background. Currents were recorded at -80 mV, in symmetrical 140 mM Cl^-; dashes on the left mark zero-current level. B-D, Mean burst (B, τ_b) and interburst (C, τ_{ib}) durations and open probabilities (D, P_o) of the six constructs in A. Red horizontal lines highlight the respective control values of the background construct. All data are shown as mean ± SEM (n = 4-28). E, Brønsted plot for position 1246. Gray symbol identifies the background construct. Solid line is a linear regression fit with slope Φ indicated.

DOI:10.14753/SE.2017.2028

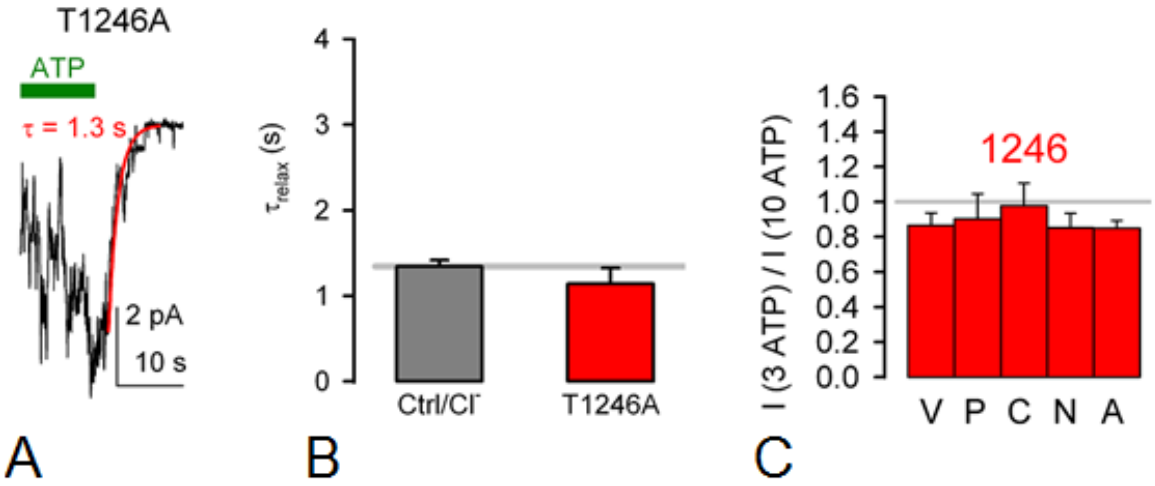

Figure 19. ATP sensitivities and macroscopic closing rates of T1246 mutants.

A, Inward macroscopic current of cut-ΔR(D1370N) CFTR harboring mutation T1246A, elicited by exposure to 10 mM MgATP (green bar). Current relaxation time course following ATP removal was fitted by a single exponential (red line) with time constant (τ) indicated.B, Macroscopic current relaxation time constant upon ATP removal for the background construct in the absence (gray bar and gray line) and presence (red bar) of the T1246A mutation. C, Fractional macroscopic currents in 3 mM ATP, normalized to the mean of the currents in the presence of bracketing applications of 10 mM ATP, for cut-ΔR(D1370N) channels harboring the indicated amino-acid substitutions (letters) at position 1246.

DOI:10.14753/SE.2017.2028

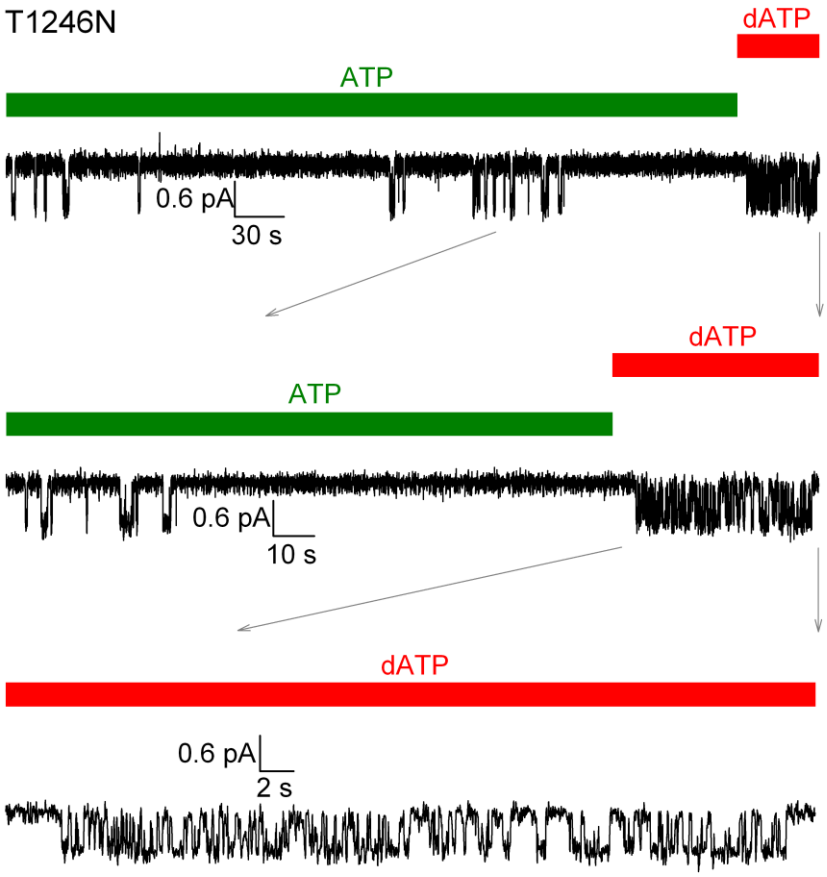

Figure 20. Stimulation of open probability by 2'-deoxy-ATP facilitates counting channels for low-P_o T1246-position mutants

Inward current of a single cut-ΔR(D1370N) channel harboring the T1246N mutation. After several minutes of low-P_o activity in 10 mM MgATP (green bar), exposure to 10 mM Mg-2'-deoxy-ATP robustly stimulated P_o. Lower panels progressively expand the timescale of indicated segments (gray arrows) of the panel above.

4.2.2. Timing of movement at the NBD2-TMD interface

Conformational changes generated by ATP binding and hydrolysis are transmitted from the nucleotide-binding to the transmembrane domains through non-covalent interactions at the shared interface. The TMDs of Sav1866 contribute to this interface mainly through the intracellular loops ICL1 and ICL2. Consistent with this finding, mutational studies and sequence comparisons indicated that the ICLs of CFTR provide similar crucial contacts[80-84]. In Sav1866, both ICLs contain short helices oriented roughly parallel to the membrane plane and providing the bulk of the contacts. These four short helices of the homodimeric transporter were named ‘coupling helices’ to emphasize their likely involvement in mechanically transmitting crucial conformational changes. Correspondingly, they are seen to undergo large movements between inward- and outward facing conformations[24, 25]. Due to domain swapping, the ICLs of Sav1866 reach across, such that coupling helix 1 contacts the NBDs of both subunits, whereas coupling helix 2 interacts with that of the opposite subunit exclusively. As confirmed by extensive cross-linking studies[81, 82], this architecture of the ICLs and coupling helices is conserved in CFTR. Thus, CH2 of TMD1 (residues 270–274) is in contact with NBD2 [82], and tyrosine 275 at the C-terminal end of CH2 is part of a conserved aromatic cluster important for NBD2-TMD interactions[85].

To test timing of motions at the NBD2-TMD transmission interface, we substituted phenylalanine, glutamate, lysine, leucine, and serine, respectively, for tyrosine 275 and studied gating of single mutant channels in 10 mM ATP (*Figure 21.A*). Perturbations at position 275 caused modest changes in P_o but in both directions (*Figures 21.A and D*). Kinetic analysis revealed a clear tendency for opposing effects on channel closing and opening rates, both contributing about equally to changes in P_o: lengthened τ_b was mostly associated with shortened τ_{ib} and (in Y275L) shortened τ_b with lengthened τ_{ib} (*Figures 21.B and 21C*).

DOI:10.14753/SE.2017.2028

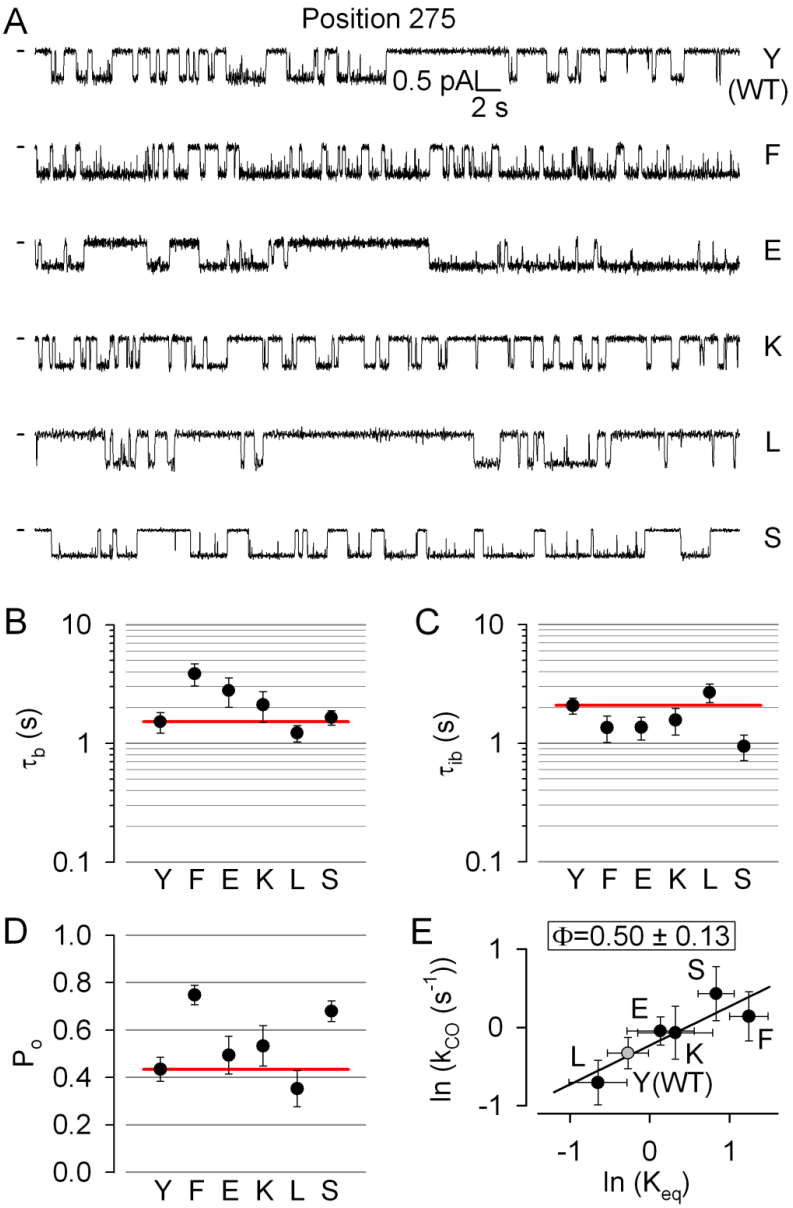

Figure 21. Timing of motion at position 275 of the NBD2-TMD interface.

A, Inward single-channel currents of the cut-ΔR(D1370N) CFTR background construct (top trace), and of channels bearing mutations Y275F, Y275E, Y275K, Y275L, and Y275S, respectively, in the same background. Currents were recorded at -80 mV, in symmetrical 140 mM Cl^-; dashes on the left mark zero-current level. B-D, Mean burst (B, τ_b) and interburst (C, τ_{ib}) durations and open probabilities (D, P_o) of the six constructs in A. Red horizontal lines highlight the respective control values of the background construct. All data are shown as mean ± SEM (n = 9-28). E, Brønsted plot for position 275. Solid line is a linear regression fit with slope Φ indicated.

Changes in opening rate ($1/\tau_{ib}$) again reflected changes in rate k_{CO} (*Figure 12.*), since 10 mM ATP remained saturating for each mutant (*Figure 22.C*). These coupled changes in opening and closing rates resulted in a Brønsted plot with an intermediate slope of Φ = 0.50 ± 0.13 (*Figure 21.E*), indicating that position 275 has not yet reached its final open-like position in the opening transition state.

4.2.3. Timing of movement within the pore region

Mutations of several pore residues were reported to affect gating[30, 33, 36, 86], indicating gating-related movements at these pore positions. To study the timing of such movements, we chose position 348 in transmembrane helix 6, because mutations here profoundly affected P_o without major effects on conductance[33], making it an attractive target for single-channel gating studies. To perturb position 348, we systematically replaced the native methionine with isoleucine, lysine, cysteine, asparagine, or alanine, and recorded single-channel currents of the mutants in 10 mM ATP (*Figure 23.A*), a saturating concentration for all constructs (*Figure 24.D*). Except for the lysine substitution, perturbations at position 348 all dramatically reduced P_o (*Figure 23.A and D*), and this effect was in every case due to speeding of closing rate (reduction in τ_b, *Figure 23.B*), with little change in opening rate ($1/\tau_{ib}$, *Figure 23.C*).

Interestingly, the M348K mutation only marginally affected gating (*Figure 23.A-D*), but increased the affinity for pore block by ATP, as reported by pronounced flickery block of single-channel currents in 10 mM ATP (*Figure 23.A*), a bell-shaped ATP dose-dependence of macroscopic currents (*Figure 24.*D, *second blue bar from left*), and a current overshoot upon ATP removal from macroscopic patches reflecting rapid unblock (*Figure 24.A*). Of note, even for M348K, the macroscopic current relaxation time constant following ATP removal (*i.e., τ_b in zero ATP; Figure 24.A; Figure 24.C, left blue bar*) remained comparable to steady-state τ_b. Thus, even pronounced flickery block of M348K by 10 mM ATP does not delay pore closure, consistent with earlier demonstration that the gate, located on the extracellular side, can readily close while large organic anion blockers remain bound in the intracellular vestibule[67].

DOI:10.14753/SE.2017.2028

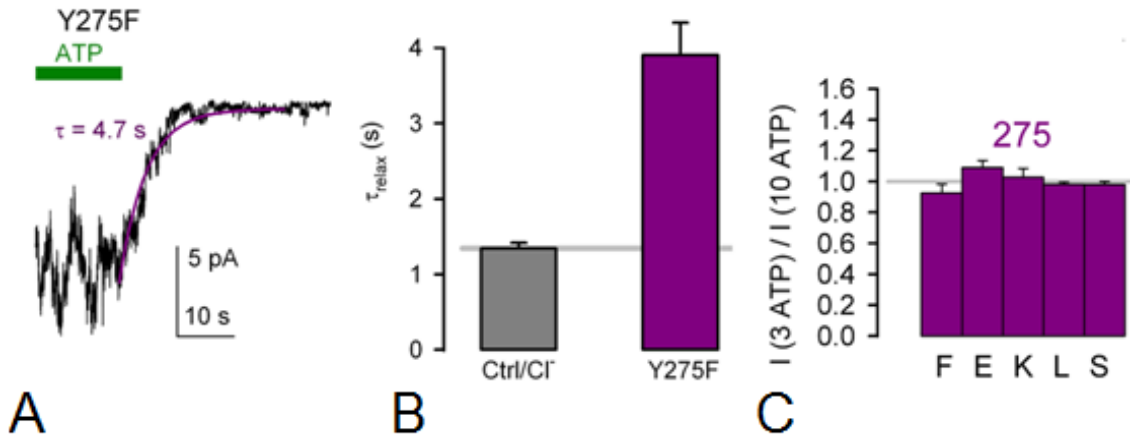

Figure 22. ATP sensitivities and macroscopic closing rates of Y275 mutants *A, Inward macroscopic current of cut-ΔR(D1370N) CFTR harboring mutation Y275F, elicited by exposure to 10 mM MgATP (green bar). Current relaxation time course following ATP removal was fitted by a single exponential (violet line) with time constant (τ) indicated. B, Macroscopic current relaxation time constant upon ATP removal for the background construct in the absence (gray bar and gray line) and presence (violet bar) of the Y275F mutation.C, Fractional macroscopic currents in 3 mM ATP, normalized to the mean of the currents in the presence of bracketing applications of 10 mM ATP, for cut-ΔR(D1370N) channels harboring the indicated amino-acid substitutions (letters) at position 275.*

DOI:10.14753/SE.2017.2028

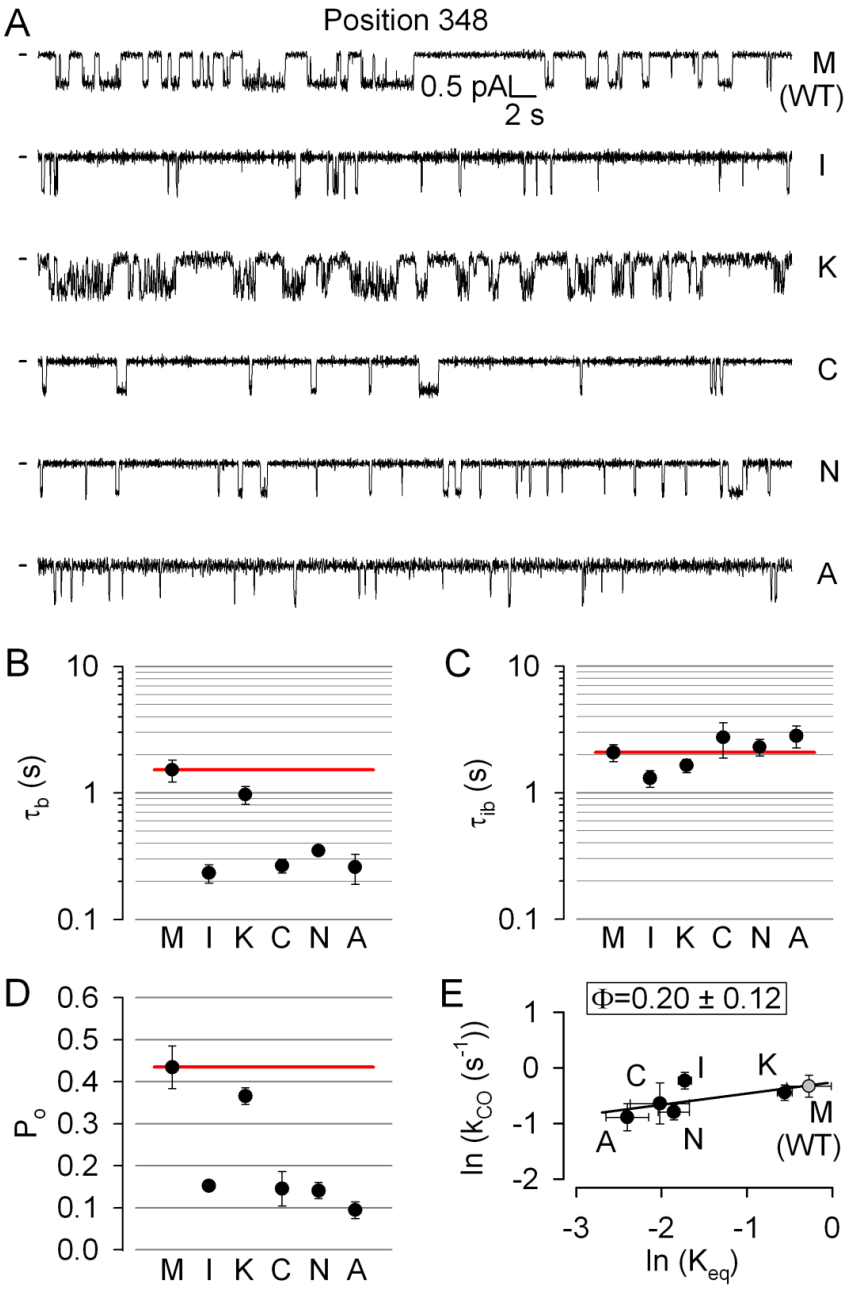

Figure 23. Timing of motion at position 348 in the pore region. *A, Inward single-channel currents of the cut-ΔR(D1370N) CFTR background construct (top trace), and of channels bearing mutations M348I, M348K, M348C, M348N, and M348A, respectively, in the same background. Currents were recorded at -80 mV, in symmetrical 140 mM Cl^-; dashes on the left mark zero-current level. B-D, Mean burst (B, τ_b) and interburst (C, τ_{ib}) durations and open probabilities (D, P_o) of the six constructs in A. Red horizontal lines highlight the respective control values of the background construct. All data are shown as mean ± SEM (n = 4-28). E, Brønsted plot for position 348. Solid line is a linear regression fit with slope Φ indicated.*

DOI:10.14753/SE.2017.2028

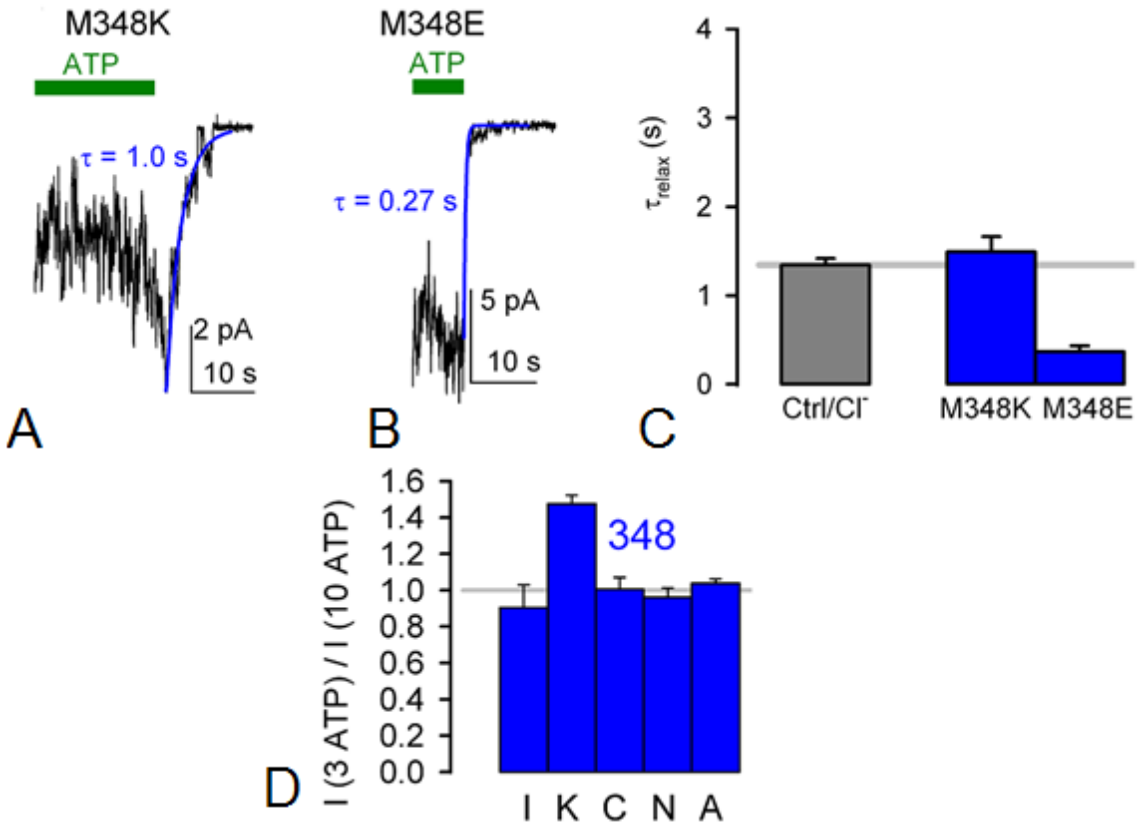

Figure 24. ATP sensitivities and macroscopic closing rates of M348 mutants

Inward macroscopic currents of cut-ΔR(D1370N) CFTR harboring mutation M348K (A) or M348E (B), elicited by exposure to 10 mM MgATP (green bar). Current relaxation time courses following ATP removal were fitted by single exponentials (blue lines) with time constants (τ) indicated. C, Macroscopic current relaxation time constant upon ATP removal for the background construct in the absence (gray bar and gray line) and presence (blue bars) of the M348K or M348E mutation.D, Fractional macroscopic currents in 3 mM ATP, normalized to the mean of the currents in the presence of bracketing applications of 10 mM ATP, for cut-ΔR(D1370N) channels harboring the indicated amino-acid substitutions (letters) at position 348.

DOI:10.14753/SE.2017.2028

We also replaced the methionine with glutamate, but this M348E mutant could not be studied at a single-channel level due to the presence of subconductance states; however, the rate of macroscopic current relaxation upon ATP removal attested to an acceleration of M348E closing rate comparable to that of the I, C, N, and A mutants (*Figure 24.E; Figure 24.C*). This speeding of non-hydrolytic closure (*step $O_1 \rightarrow C_1$ in Figure 12., rate k_{OC}*) by perturbations at position 348, with little effect on opening rate, led to a Brønsted plot with a small slope of Φ=0.20±0.12 (*Figure 23.E*), indicating that this pore region still resembles its closed-state conformation in the opening transition state.

4.2.4. Timing of movements in the narrow region of the pore studied by anion substitution

Previous accessibility studies outlined a short narrow region of the pore, confined to approximately one helical turn of pore-forming transmembrane helices 1 (residues 102-106), 6 (residues 337-341), 11 (residues 1115-1118), and 12 (residues 1130-36)[30-34, 36, 37]. This narrow region was shown to act as a lyotropic "selectivity filter" which provides sites of interaction (T338, S341, S1118, T1134) for permeating anions[87-89]. Intriguingly, replacement of chloride with nitrate affects CFTR gating[90], suggesting that interactions of permeating anions with residues lining the "filter" region of the open pore energetically contribute to open-state stability. Thus, replacement of chloride with other permeant anions might be viewed as a structural perturbation of the "selectivity filter".

We therefore studied changes in the pattern of single-channel gating of our background construct cut-ΔR(D1370N) in response to sudden replacement of cytosolic chloride with nitrate, bromide, or formate. Of note, in these experiments gating in chloride and in the replacement anion could be compared within the same patch (*Figure 25.A*).

DOI:10.14753/SE.2017.2028

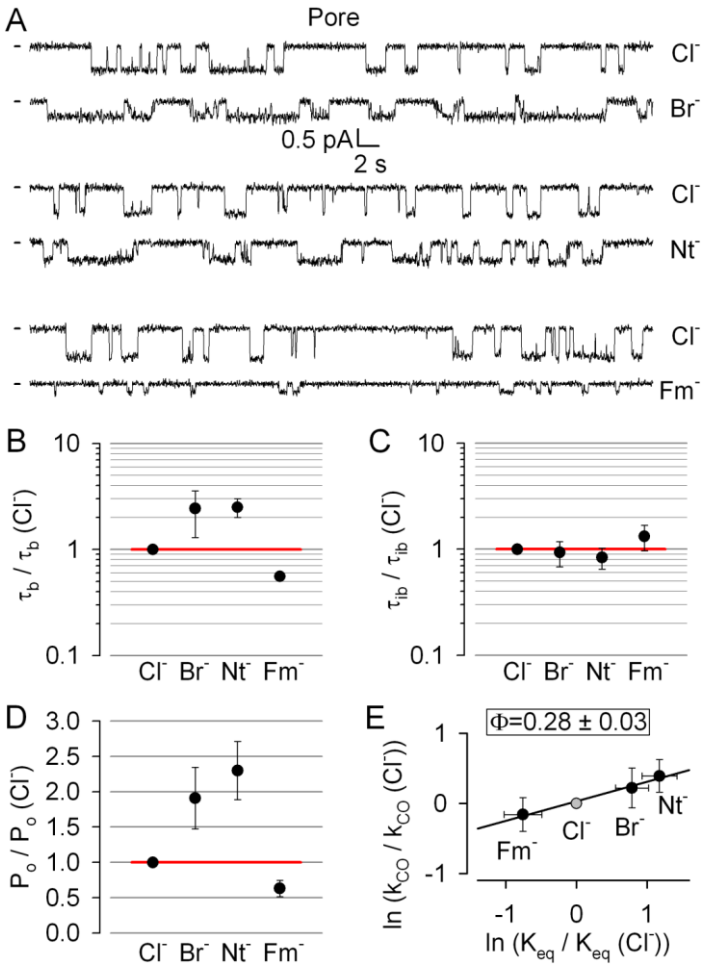

Figure 25. Timing of motion in the narrow region of the pore studied by anion replacement.

A, Pairs of segments of inward single-channel current from three patches containing single cut-ΔR(D1370N) CFTR channels. Each patch was alternately exposed to bath solutions containing 140 mM of either chloride (upper segments) or a test anion (lower segments), as indicated to the right: chloride (Cl^-), bromide (Br^-), nitrate (Nt^-), formate (Fm^-). Currents in Cl^-, Br^-, and Nt^- were recorded at -80 mV, those in Fm^- at -100 mV; dashes on the left mark zero-current level. B-D, Mean burst (B, τ_b) and interburst (C, τ_{ib}) durations and open probabilities (D, P_o) in the presence of various test anions, each normalized to the value observed in chloride in the same patch. Red horizontal lines highlight the respective control values in chloride. All data are shown as mean ± SEM (n = 5-9). E, Brønsted plot for the narrow region of the pore, constructed from normalized opening rates and equilibrium constants in the presence of the four permeating anions tested. Solid line is a linear regression fit with slope Φ indicated.

DOI:10.14753/SE.2017.2028

The latter arrangement eliminates any uncertainties about perturbation-induced fractional changes in opening rate, precise estimation of which is normally dependent on correct judgment of the number of active channels in each patch. In addition to documented reductions in unitary conductance[88], perturbations of the filter by replacement of permeating chloride with nitrate, bromide, or formate all affected gating: nitrate and bromide which bind more tightly in the pore[88] increased P_o, while formate which binds less tightly[88] decreased it (*Figure 25.A and D*). Importantly, both gating effects primarily reflected changes in τ_b (*Figure 25.B*), i.e., in rate k_{OC} of step $O_1 \rightarrow C_1$ (*Figure 12.*), with smaller changes in τ_{ib} (*Figure 25.C*); the observations on nitrate replicated those of[90]. The slope of the Brønsted plot constructed from these data yielded $\Phi = 0.28 \pm 0.03$ (*Figure 25.E*), similar to that of position 348. Of note, the observed changes in τ_b were confirmed by measurements of cut-ΔR(D1370N) macroscopic closing rate in the presence of the three test anions (*Figure 26.*). These ionic replacement studies therefore provide independent support for a small Φ value in the pore, confirming late movement of this region during opening.

DOI:10.14753/SE.2017.2028

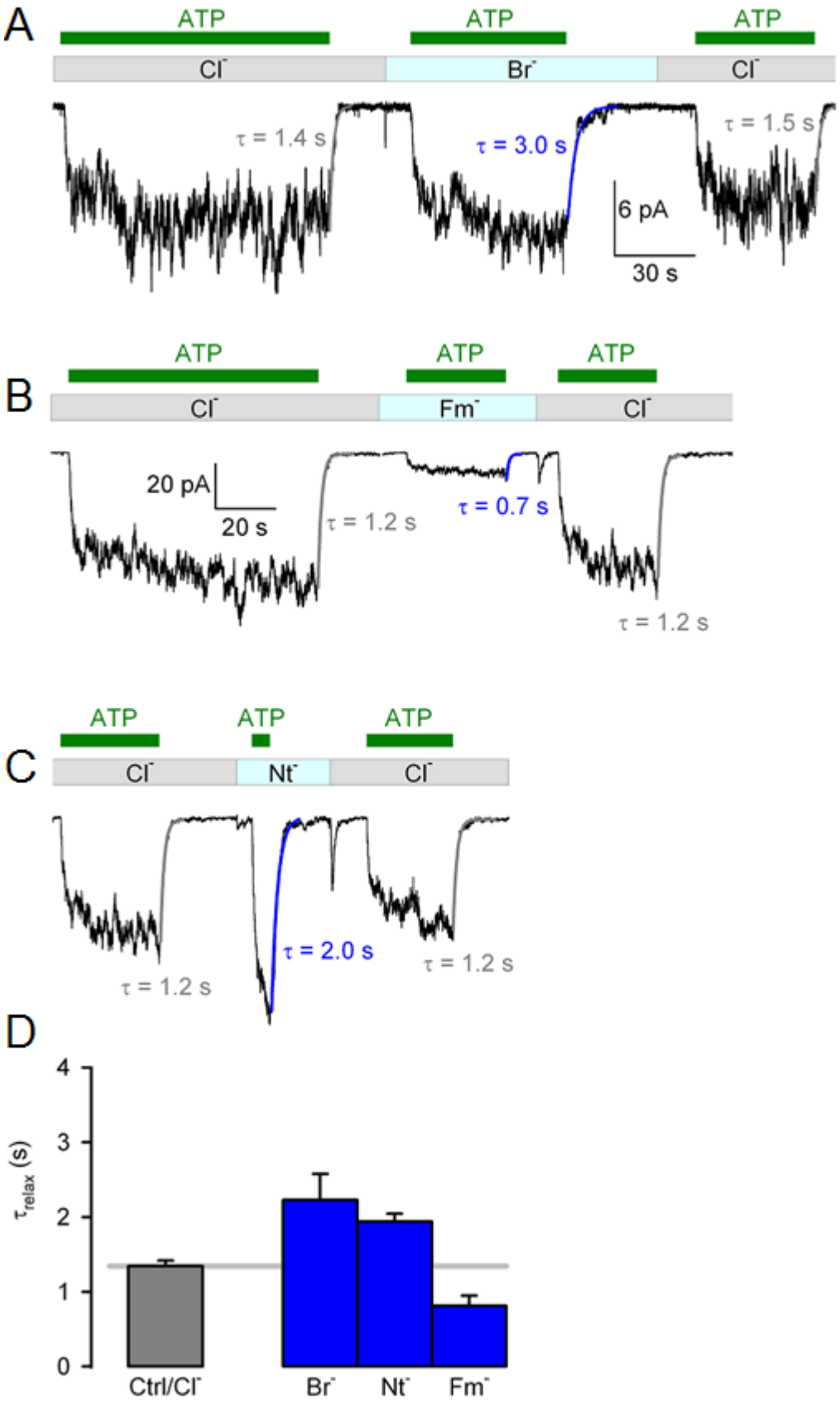

DOI:10.14753/SE.2017.2028

Figure 26. Cut-ΔR(D1370N) macroscopic closing rates in the presence of various bath anions

Inward macroscopic currents of cut-ΔR(D1370N) CFTR evoked by repetitive exposures to 10mM ATP in the alternating presence of various bath anions (gray/light-blue bars: chloride (Cl^-); bromide (Br^-); formate (Fm^-) ; nitrate (Nt^-)). .

All recordings were obtained at -80 mV; all current relaxation time courses following ATP removal were fitted by single exponentials (colored solid lines) with time constants (τ) indicated (A-C, chloride (Cl^-); A, bromide (Br^-); B, formate (Fm^-) C, nitrate (Nt^-)). D, Macroscopic current relaxation time constants for cut-ΔR(D1370N) upon ATP removal in the presence of either chloride (gray bar) or the specified anion (blue bars) in the bath. All data are shown as mean ± SEM (n = 2-9), gray line highlights the control value in chloride.

DOI:10.14753/SE.2017.2028

5. Discussion

The general structural orientations of protein domains in the stable closed and open states of the CFTR channel have been delineated by a large body of previous work. Thus, the preponderance of evidence has established that the channel's closed state corresponds to a dissociated NBD dimer interface[20, 91, 92] and inward-facing TMDs[46-48], with the closed gate located on the extracellular side of the membrane[46, 47, 67, 93]. Similarly, evidence suggests that in the open state the NBDs are dimerized[20, 91, 92], while a conducting pore is formed by outward-facing TMDs[46-48]. Consequently, several homology models of closed- and open-state CFTR have been constructed based on crystal structures of homologous ABC exporters in their inward- and outward-facing conformations (*e.g. [42] and [40]; Figure 27., left and right ribbon representations respectively*). In contrast, far less is known about the nature and relative timing of the sub-microsecond molecular motions that drive the channel from its closed- to its open-state conformation.

Here we have adapted the REFER technique to obtain new insight into the dynamics of ATP-dependent gating conformational changes of the CFTR protein: careful choice of the background construct (see below) allowed selective examination of the channel opening process (*step $C_1 \rightarrow O_1$, Figure 12.*). The strikingly different Φ values obtained for our three target positions define a clear spatial gradient along the protein's longitudinal axis from cytoplasm to cell exterior: the very high Φ value of ~0.97 for site-2 NBD interface position 1246 (*Figure 18.E, Figure 28., red*) stands in stark contrast to the low Φ value of ~0.20 for intra-pore position 348. For the pore region a similarly small Φ value emerges also from our anion substitution studies: replacement of permeating chloride with anions such as nitrate and bromide, which bind more tightly to the pore (as indicated by permeability ratio measurement[88]), clearly stabilize the open state, whereas formate, which binds less tightly than chloride[88], destabilizes it (*Figure 25.D*).

DOI:10.14753/SE.2017.2028

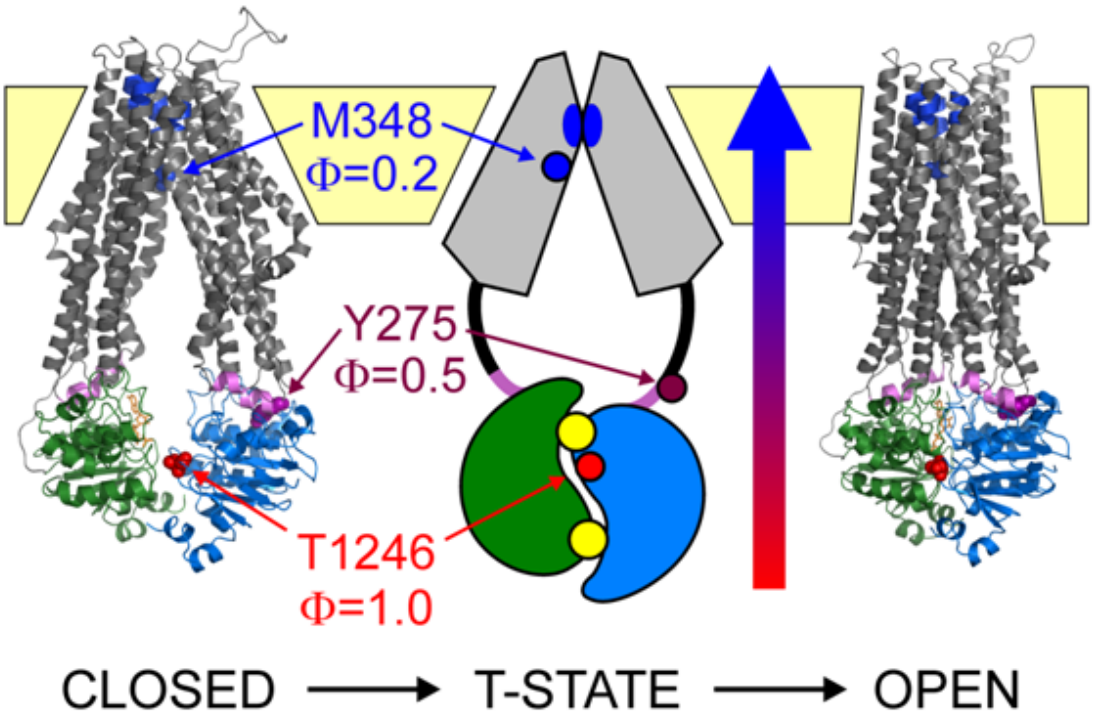

Figure 27. Opening conformational wave and transition-state structure reported by Φ-value analysis.

Ribbon representation of CFTR homology models[40] in the closed (left) and open (right) states based on (left) the inward-facing structure of TM287-288[25] and (right) the outward-facing structure of Sav1866[24]), and cartoon depicting rough domain organization in the opening transition state (center). The three target positions are highlighted in spacefill on the models, and as colored circles in the cartoon. CFTR domain color coding follows that of Figs. 12-13; threonine 1246 (red), tyrosine 275 (violet), methionine 348 (blue). Blue ribbons in the homology models highlight segments 102-106 (TM1), 337-341 (TM6), 1115-1118 (TM11), and 1130-1134 (TM12), that form the narrow region of the pore (blue ovals in cartoon). Vertical colored arrow illustrates the direction and timing of the conformational wave during pore opening (early – red, late – blue).

DOI:10.14753/SE.2017.2028

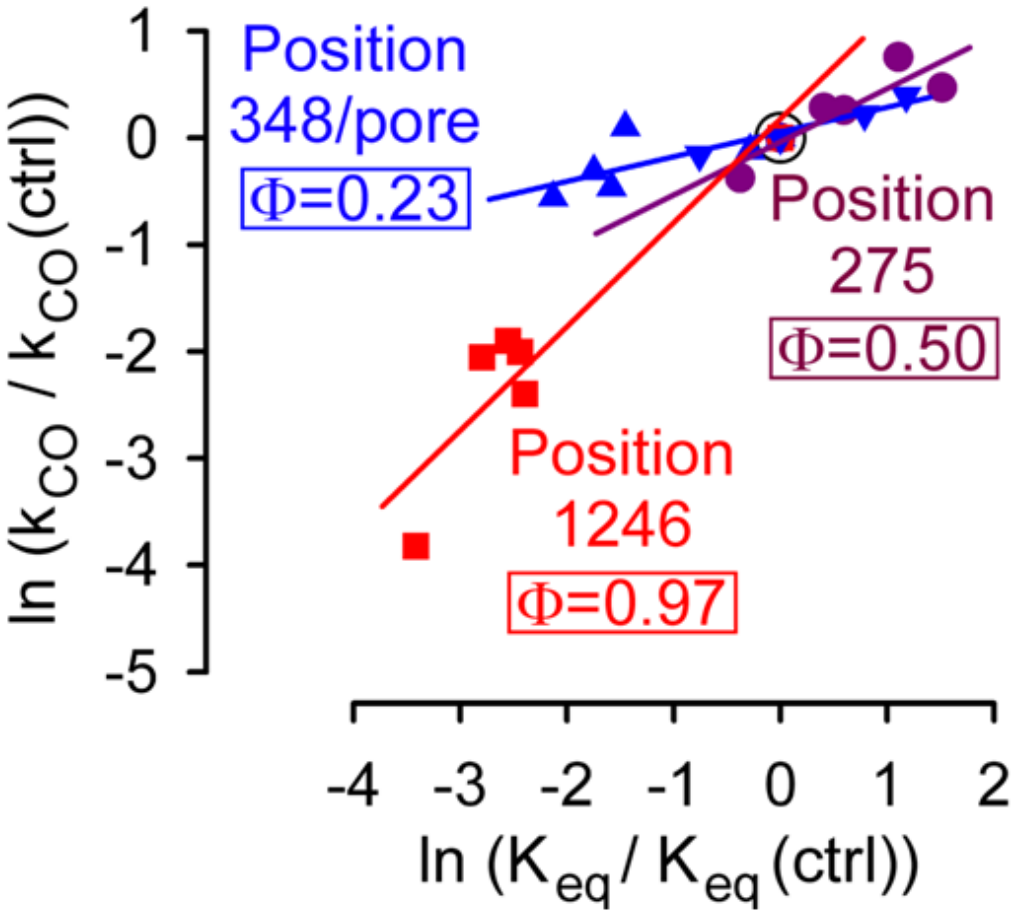

Figure 28. Comparison of normalized Brønsted plots of the three regions

Merged normalized Brønsted plot for the pore region (blue). Fitting the ensemble of the normalized data for position 348 (standing triangles) and for the anion substitution experiments (inverted triangles) by linear regression (solid blue line) yielded the indicated slope value (Φ). Brønsted plots for positions 1246 (red) and 275 (violet) are normalized versions of the plots in Figures 18.E and 21.E, respectively. The point representing the cut-ΔR(D1370N) background construct in chloride is highlighted by a black circle.

Although the precise location at which permeating anions act to affect CFTR gating is unknown, this strong positive correlation between anion binding affinity in the filter and open-state stability does support the notion that the gating effects are caused by interactions of the anions with residues located somewhere in the pore. It is notable that the effects of ionic replacement on open-closed equilibrium were in each case associated with changes in closing, rather than opening rates (*Figure 25.B and C*), implying that the stability of the transition state, relative to the closed state, is less sensitive to the permeating anion species. Insofar as pore-anion interactions are expected to change between the closed and open state, the implication is that in the transition state these interactions resemble those in the closed state: i.e., the pore is closed. The Brønsted plots for ionic replacement and for the 348 position closely agree with each other, and the combined data are well fitted by a single line with a slope of 0.23±0.05 (*Figure 28., blue*). Compared to the Φ values for the NBD1-NBD2 interface and the pore, which are close to the smallest and highest possible values for this parameter, respectively, the slope of ~0.50 of the Brønsted plot for NBD-TMD interface position 275 (*Figure 28., violet*) appears intermediate, distinctly different from the two extremes. This spatially organized Φ value gradient provides support for the interpretation that for conformational changes of folded proteins the relative magnitude of Φ reflects relative timing of ordered sequential movements[51, 52], albeit on the sub-microsecond time scale, as opposed to probabilities of taking alternative kinetic pathways known to exist for more random processes such as protein folding (cf.,[58]). For the CFTR pore opening transition this spatial Φ-gradient implies a conformational wave (*Figure 27., large vertical arrow*) initiated by tightening of the NBD dimer around site 2, and propagated with some delay through the NBD-TMD interface to eventually result in pore opening.

Furthermore, this set of Φ values provides strong global constraints for the structure of the actual transition state, the highest free-energy intermediate of the channel opening process (*Figure 27., center*). For the NBD interface the Φ value of ~1 indicates that it has already reached its open-state conformation, i.e., the tight dimer is already formed (cf.,[20]). In contrast, the low Φ value of ~0.2 for the pore region implies it is still in its closed-like, inward-facing conformation. Finally, the intermediate Φ value of ~0.5 for position 275 suggests that in the transition state coupling helix 2 is

just on the move: it has already left its closed-like, but has not yet reached its open-like conformation (*Figure 27., center, bent rods*). This transition state architecture, which emerges from direct measurements of relative timing of movements, confirms a previous speculation based on interpretation of enthalpy and entropy changes determined for the opening transition state[94], but refutes the alternative proposition that during opening all structural reorganizations in the cytoplasmic loops are completed in the channel closed state[61]. The large molecular strain which must arise at the NBD-TMD interface is the most likely cause of the very high enthalpy of the opening transition state ($\Delta H^{\ddagger}$ =117 kJ/mol), and is only partially compensated by an entropy increase ($T\Delta S^{\ddagger} \geq 41$ kJ/mol) suggested to reflect dehydration of the closing NBD dimer interface (i.e., dispersal of the layer of ordered water molecules into the disordered bulk solution)[94]. Evidently, transition-state free energy ($\Delta G^{\ddagger} = \Delta H^{\ddagger} - T\Delta S^{\ddagger}$) of wild-type CFTR is still very high, as witnessed by its very slow opening rate of ~1 s^{-1}, >4 orders of magnitude slower than for the ligand-gated nicotinic acetylcholine receptor (e.g.,[95]). Moreover, it is this transient conformation of CFTR which is further destabilized (relative to the closed state) by NBD-TMD interface mutation ΔF508, causing the severe gating defect of this most common CF-associated mutant. Indeed, stabilization of the opening transition state seems an attractive strategy for designing potentiator compounds that stimulate gating of ΔF508 CFTR: thus, 5-Nitro-2-(3-phenylpropylamino)benzoate, one of its most efficacious potentiators (albeit with a pore blocking side effect; [67]), increases ΔF508 CFTR opening rate by precisely that mechanism[67]. Successful adaptation of the classical REFER approach to studying CFTR gating dynamics rested on three important innovations.

First, rather than focusing on the kinetics of pore opening and closure (cf.,[62]), the durations of *bursts* of openings and of long *interburst* closures were analyzed here, as the latter reflect conformational states of the pore associated with specific conformations of the NBDs: bursts are linked to tightly dimerized NBDs, while interburst closures reflect dissociation of the NBD interface around site 2[20, 92]. The duration of the "active" pore conformation induced by a single ATP occlusion event at site 2 is also reflected by the time constant of macroscopic current relaxation upon sudden removal of ATP. Indeed, for all of our constructs which afforded macroscopic recordings, such macroscopic current relaxation time constants (*Figures 19., 22., 24.*,

26.) were in good agreement with the mean burst durations obtained by conventional burst analysis of steady-state single-channel recordings (*Figures 18.B, 21.B, 23.B, 25.B*), confirming that τ_b indeed reflects the duration of an activated state of the pore induced by a single ATP occlusion event.

Second, CFTR bursting follows a non-equilibrium cycle[49, 96] (*cf., Figure 7.*) to which REFER analysis is not applicable[55]. To study the pore opening step, we therefore employed the D1370N background mutation which truncates the gating cycle to an equilibrium scheme (*Figure 12., red frame*). Indeed, this is the key feature which distinguishes our approach from previous studies, and is responsible for its very different outcome. This is because in the normal hydrolytic background, mutation-induced changes in the rate of slow non-hydrolytic closure (rate k_{OC}, *Figure 7.*) remain unnoticed as long as the much faster hydrolytic pathway (*rate* $O_1 \rightarrow O_2$, *Figure 7.*) dominates pore closure. It is therefore not surprising that structural perturbations introduced into the nucleotide binding sites and several TMD/NBD interface positions of WT CFTR affected only channel opening rates, yielding apparent Φ values of ~1 for all positions tested[61]. Similarly, previous studies identified several pore mutations that affected gating[30, 33], but in the framework of a hydrolytic gating cycle even the large, almost an order of magnitude, acceleration of non-hydrolytic closing rates reported here for mutations at position 348 so far evaded detection. Of note, the ΔF508 mutation also greatly accelerates non-hydrolytic closure[97]– suggesting an intermediate Φ value for position 508 –, yet under normal hydrolytic conditions ΔF508 closing rate is unaffected[66, 98].

Third, removal of the R domain eliminated potential confounding effects of altered R-domain mediated gating regulation in our target-site mutants: not only does the non-phosphorylated R domain *inhibit* channel gating, but the phosphorylated R domain also mediates substantial *stimulation* of channel $P_{o[69, 99]}$, through mechanisms which are poorly understood. In that regard our cut-ΔR background construct, pared down to the canonical ABC domains, reduces complexity: in addition to obviating the need for prior phosphorylation by PKA, gating of cut-ΔR CFTR is regulated only by ATP, similarly to the transport cycle of ABC exporters. Thus, our Φ-value map likely bears relevance to the transition state for the inward- to outward-facing transition in this broader family of CFTR relatives. Because gating of cut-ΔR(D1370N), like that of WT

CFTR, is strictly ATP dependent (*Figures 15. and 16.*), our conclusions do not necessarily apply to the mechanism of the extremely infrequent spontaneous openings observable in the absence of ATP that are promoted by certain mutations[64] and drugs[100].

In conclusion, we have provided an initial characterization of the CFTR opening transition-state structure which could serve as a drug target for treating CF, and developed a technique to directly measure timing of movements in distinct regions of the CFTR protein during the sub-microsecond process of channel opening. By further refining the Φ value map, this approach might be used in the future to define regions which move as a rigid body[57, 58], or to shed light on potentially asynchronous movements at the level of the ATP binding sites, the coupling helices, or the TM helices that form the pore.

6. Conclusions

- CFTR cut-ΔR(D1370N), obtained by coexpression of CFTR segments 1-633 and 837-1480(D1370N) in *Xenopus laevis* oocytes, is active in the absence of phosphorylation and gates in a strictly ATP-dependent manner.

- In the presence of saturating ATP the ATP-dependent slow gating process of CFTR cut-ΔR(D1370N) is reduced to a two-state equilibrium mechanism, suitable for Rate Equilibrium Free Energy Relationship (REFER) analysis.

- Mutations of position 1246 in the NBD2 Walker A motif (composite site 2) affect opening, but not closing rate of cut-ΔR(D1370N).

- Mutations of position 275 in coupling helix 2 affect both opening and closing rate of cut-ΔR(D1370N), but in opposite directions.

- Mutations of position 348 in TM6 affect primarily closing, but not opening rate of cut-ΔR(D1370N).

- Substitution of permeating chloride ions for nitrate, bromide, or formate affect primarily closing, but not opening rate of cut-ΔR(D1370N).

- The pore opening conformational change is initiated at the site-2 NBD interface, and is propagated along the longitudinal protein axis towards the pore.

- In the transition state for pore opening the site-2 NBD interface is already tightened, but the pore is still closed, creating strain at the NBD-TMD interface which contains disease locus F508.

DOI:10.14753/SE.2017.2028

7. Summary

In CFTR, the chloride ion channel mutated in cystic fibrosis (CF) patients, pore opening is coupled to ATP binding-induced dimerization of two cytosolic nucleotide binding domains (NBDs), and closure to dimer disruption following ATP hydrolysis. CFTR opening rate is unusually slow because of its high-energy transition state, and is further slowed by CF mutation ΔF508. Here we exploit equilibrium gating of hydrolysis-deficient CFTR mutant D1370N, and lack of phosphorylation-dependence of R-domain deleted (cut-ΔR) channels, to apply Rate-Equilibrium Free Energy Relationship analysis for the estimation of relative timing of opening movements in distinct protein regions of cut-ΔR(D1370N) CFTR. We introduced five mutations into each of three different positions in our background construct, recorded channel gating in inside-out patches to compare the gating patterns at a single-molecule level, and constructed Brønsted plots. The slope Φ ($0 \leq \Phi \leq 1$) of such plots reports relative timing of movement in the tested position. Upon pore opening: Φ=1 indicates that the test position has already reached its open-like conformation, whereas Φ=0 implies it is still in its closed-like conformation, in the opening transition state. An intermediate Φ value (Φ~0.5) implies that the position is just on the move in the transition state. The strikingly different Φ values obtained for our three target positions define a clear spatial gradient along the protein's longitudinal axis from cytoplasm to cell exterior: the very high Φ value of ~1.0 for site-2 NBD interface position 1246 stands in stark contrast to the low Φ value of ~0.2 for both the intra-pore posi-tion 348 and for another Brønsted plot of the pore region, obtained from anion substitution studies (replacement of permeating chloride with other anions). Compared to these extreme Φ values, Φ~0.5 for the NBD-TMD interface position 275 appears intermediate. Hence, we found clear directionality of motion along the longitudinal protein axis, and identified an opening transition-state structure with the NBD dimer formed but the pore still closed. Thus, strain at the NBD/pore-domain interface, the ΔF508 mutation locus, underlies the energetic barrier for opening. Our findings suggest a therapeutic opportunity to stabilize this transition-state structure pharmacologically in ΔF508-CFTR to correct its opening defect, an essential step toward restoring CFTR function.

DOI:10.14753/SE.2017.2028

8. Összefoglalás

A cisztikus fibrózis (CF) betegekben sérült CFTR klorid ioncsatorna pórusát két citoszolikus nukleotidkötő domén (NBD) ATP-kötést követő dimerizációja nyitja meg, és a dimer ATP-hidrolízist követő szétesése zárja be. A CFTR szokatlanul lassú nyitási sebességét a nyitási átmeneti állapot magas szabadentalpiája okozza, és a ΔF508 CF mutáció tovább csökkenti. Az ATP-hidrolízisre képtelen D1370N mutáns egyensúlyi kapuzását és az R-domén-deletált (cut-ΔR) csatornák foszforiláció-függetlenségét kihasználva Rate-Equilibrium Free Energy Relationship (REFER) módszer segítségével vizsgáltuk a pórusnyitás során a különböző fehérje régiók mozgásainak viszonylagos sorrendjét. R-doménmentes D1370N háttérkonstrukciónk három különböző pozíciójának mindegyikébe öt-öt mutációt vittünk be, egy-csatornás membránfoltokban regisztráltuk mindegyik mutáns kapuzási mintázatát, és Brønsted grafikonokat szerkesztettünk. E grafikonok Φ meredeksége ($0 \leq \Phi \leq 1$) a tesztpozíció mozgásainak időzítését tükrözi: Φ=1 arra utal, hogy az átmeneti állapotban a pozíció már elérte nyitott állapotra jellemző lokális konformációját, míg Φ=0 esetén a pozíció még a zárt állapotára jellemző konformációban van. Átmeneti Φ érték (Φ~0.5) jellemzi azon régiókat, amelyek az átmeneti állapotban éppen mozgásban vannak. Három tesztpozíciónk merőben különböző Φ értékei a fehérje hossztengelye mentén a citoszol felől az extracelluláris tér irányába mutató markáns térbeli gradienst körvonalaznak: az NBD érintkezési felszín 2-es kötőhelyében tlálható 1246-os pozíció nagyon magas, 1 körüli Φ értéke erős kontrasztban áll a pórusrégiót jellemző alacsony, 0.2 körüli, Φ értékkel amelyet mind a 348-as póruspozíció, mind anion helyettesítéses kísérletek Brønsted grafikonjai sugallnak. E szélsőséges Φ értékekhez képest az NBD-TMD határfelszín 275-ös pozíciójának 0.5 körüli Φ értéke átmenetinek bizonyult. Ezen eredmények a mozgások hossztengely menti irányítottságáról tanúskodnak, és rámutatnak arra, hogy a nyitási átmeneti állapotban az NBD dimer már kialakult, de a pórus még zárt. Tehát, a ΔF508 mutáció helyét tartalmazó NBD-TMD érintkezési felszínek feszülése okozza a nyitási lépés magas aktivációs szabadentalpiáját. Eredményeink terápiás lehetőségként azonosítják ezen átmeneti szerkezet gyógyszeres stabilizálását a ΔF508 mutánsban, ezáltal növelve annak csökkent nyitási sebességét: ez elengedhetetlenül fontos lenne a csökkent CFTR működés helyreállításához.

9. Bibliography

1. O'Sullivan, B.P. and S.D. Freedman. (2009) *Cystic fibrosis.* Lancet,. **373**(9678): p. 1891-904.
2. Thiagarajah, J.R. and A.S. Verkman. (2005) *New drug targets for cholera therapy.* Trends Pharmacol Sci,. **26**(4): p. 172-5.
3. Dean, M. and T. Annilo (2005) *Evolution of the ATP-binding cassette (ABC) transporter superfamily in vertebrates.* Annu Rev Genomics Hum Genet,. **6**: p. 123-42.
4. Locher, K.P. (2009) *Review. Structure and mechanism of ATP-binding cassette transporters.* Philos Trans R Soc Lond B Biol Sci,. **364**(1514): p. 239-45.
5. Jones, P.M. and A.M. George. (2004) *The ABC transporter structure and mechanism: perspectives on recent research.* Cell Mol Life Sci,. **61**(6): p. 682-99.
6. Tomii, K. and M. Kanehisa. (1998) *A comparative analysis of ABC transporters in complete microbial genomes.* Genome Res,. **8**(10): p. 1048-59.
7. Dean, M., A. Rzhetsky, and R. Allikmets. (2001) *The human ATP-binding cassette (ABC) transporter superfamily.* Genome Res,. **11**(7): p. 1156-66.
8. Vasiliou, V. (2009) *The exact mechanism of ethanol-associated carcinogenesis still remains unknown, a number of factors may contribute to the development of alcohol-associated cancer, including ethanol metabolising enzymes. Editorial.* Hum Genomics,. **3**(2): p. 101-2.
9. Wilkens, S. (2015) *Structure and mechanism of ABC transporters.* F1000Prime Rep,. **7**: p. 14.
10. Rees, D.C., E. Johnson, and O. Lewinson (2009) *ABC transporters: the power to change.* Nat Rev Mol Cell Biol,. **10**(3): p. 218-27.
11. Hung, L. W., Wang, I. X., Nikaido, K., Liu, P. Q., Ames, G. F., and Kim, S. H. (1998) *Crystal structure of the ATP-binding subunit of an ABC transporter.* Nature,. **396**(6712): p. 703-7.
12. Diederichs, K., Diez, J., Greller, G., Muller, C., Breed, J., Schnell, C., Vonrhein, C., Boos, W., and Welte, W. (2000) *Crystal structure of MalK, the ATPase subunit of the trehalose/maltose ABC transporter of the archaeon Thermococcus litoralis.* EMBO J. **19**(22): p. 5951-61.
13. Pohl, A., P.F. Devaux, and A. Herrmann. (2005) *Function of prokaryotic and eukaryotic ABC proteins in lipid transport.* Biochim Biophys Acta. **1733**(1): p. 29-52.
14. Dawson, R.J. and K.P. Locher. (2007) *Structure of the multidrug ABC transporter Sav1866 from Staphylococcus aureus in complex with AMP-PNP.* FEBS Lett. **581**(5): p. 935-8.
15. Schneider, E. and S. Hunke. (1998) *ATP-binding-cassette (ABC) transport systems: functional and structural aspects of the ATP-hydrolyzing subunits/domains.* FEMS Microbiol Rev. **22**(1): p. 1-20.
16. Hopfner, K. P., Karcher, A., Shin, D. S., Craig, L., Arthur, L. M., Carney, J. P., and Tainer, J. A. (2000) *Structural biology of Rad50 ATPase: ATP-driven conformational control in DNA double-strand break repair and the ABC-ATPase superfamily.* Cell. **101**(7): p. 789-800.
17. Smith, P. C., Karpowich, N., Millen, L., Moody, J. E., Rosen, J., Thomas, P. J., and Hunt, J. F. (2002) *ATP binding to the motor domain from an ABC*

transporter drives formation of a nucleotide sandwich dimer. Mol Cell. **10**(1): p. 139-49.

18. Hrycyna, C. A., Ramachandra, M., Ambudkar, S. V., Ko, Y. H., Pedersen, P. L., Pastan, I., and Gottesman, M. M. (1998) *Mechanism of action of human P-glycoprotein ATPase activity. Photochemical cleavage during a catalytic transition state using orthovanadate reveals cross-talk between the two ATP sites.* J Biol Chem,. **273**(27): p. 16631-4.
19. Chen, J., Sharma, S., Quiocho, F. A., and Davidson, A. L. (2001) *Trapping the transition state of an ATP-binding cassette transporter: evidence for a concerted mechanism of maltose transport.* Proc Natl Acad Sci U S A. **98**(4): p. 1525-30.
20. Vergani, P., Lockless, S. W., Nairn, A. C., and Gadsby, D. C. (2005) *CFTR channel opening by ATP-driven tight dimerization of its nucleotide-binding domains.* Nature. **433**(7028): p. 876-80.
21. Senior, A.E. and S. Bhagat. (1998) *P-glycoprotein shows strong catalytic cooperativity between the two nucleotide sites.* Biochemistry. **37**(3): p. 831-6.
22. Verdon, G., Albers, S. V., van Oosterwijk, N., Dijkstra, B. W., Driessen, A. J., and Thunnissen, A. M. (2003) *Formation of the productive ATP-Mg2+-bound dimer of GlcV, an ABC-ATPase from Sulfolobus solfataricus.* J Mol Biol **334**(2): p. 255-67.
23. Janas, E., Hofacker, M., Chen, M., Gompf, S., van der Does, C., and Tampe, R. (2003) *The ATP hydrolysis cycle of the nucleotide-binding domain of the mitochondrial ATP-binding cassette transporter Mdl1p.* J Biol Chem. **278**(29): p. 26862-9.
24. Dawson, R.J. and K.P. Locher. (2006) *Structure of a bacterial multidrug ABC transporter.* Nature. **443**(7108): p. 180-5.
25. Hohl M, Briand C, Grütter MG, and Seeger MA. (2012) *Crystal structure of a heterodimeric ABC transporter in its inward-facing conformation.* Nat Struct Mol Biol. **19**(4): p. 395-402.
26. Aller, S. G., Yu, J., Ward, A., Weng, Y., Chittaboina, S., Zhuo, R., Harrell, P. M., Trinh, Y. T., Zhang, Q., Urbatsch, I. L., and Chang, G. (2009) *Structure of P-glycoprotein reveals a molecular basis for poly-specific drug binding.* Science,. **323**(5922): p. 1718-22.
27. Ward, A., Reyes, C. L., Yu, J., Roth, C. B., and Chang, G. (2007) *Flexibility in the ABC transporter MsbA: Alternating access with a twist.* Proc Natl Acad Sci U S A. **104**(48): p. 19005-10.
28. Riordan, J. R., Rommens, J. M., Kerem, B., Alon, N., Rozmahel, R., Grzelczak, Z., Zielenski, J., Lok, S., Plavsic, N., and Chou, J. L. (1989) *Identification of the cystic fibrosis gene: cloning and characterization of complementary DNA.* Science. **245**(4922): p. 1066-73.
29. Bear, C. E., Li, C. H., Kartner, N., Bridges, R. J., Jensen, T. J., Ramjeesingh, M., and Riordan, J. R. (1992) *Purification and functional reconstitution of the cystic fibrosis transmembrane conductance regulator (CFTR).* Cell. **68**(4): p. 809-18.
30. Beck, E. J., Yang, Y., Yaemsiri, S., and Raghuram, V. (2008) *Conformational changes in a pore-lining helix coupled to cystic fibrosis transmembrane conductance regulator channel gating.* J Biol Chem. **283**(8): p. 4957-66.
31. Fatehi, M. and P. Linsdell (2009) *Novel residues lining the CFTR chloride channel pore identified by functional modification of introduced cysteines.* J Membr Biol. **228**(3): p. 151-64.

32. El Hiani, Y. and P. Linsdell. (2010)*Changes in accessibility of cytoplasmic substances to the pore associated with activation of the cystic fibrosis transmembrane conductance regulator chloride channel.* J Biol Chem. **285**(42): p. 32126-40.
33. Bai, Y., M. Li, and T.C. Hwang (2010) *Dual roles of the sixth transmembrane segment of the CFTR chloride channel in gating and permeation.* J Gen Physiol. **136**(3): p. 293-309.
34. Qian, F., Y. El Hiani, and P. Linsdell (2011) *Functional arrangement of the 12th transmembrane region in the CFTR chloride channel pore based on functional investigation of a cysteine-less CFTR variant.* Pflugers Arch. **462**(4): p. 559-71.
35. Wang, W., Y. El Hiani, and P. Linsdell (2011) *Alignment of transmembrane regions in the cystic fibrosis transmembrane conductance regulator chloride channel pore.* J Gen Physiol. **138**(2): p. 165-78.
36. Gao, X., Y. Bai, and T.C. Hwang (2013) *Cysteine scanning of CFTR's first transmembrane segment reveals its plausible roles in gating and permeation.* Biophys J. **104**(4): p. 786-97.
37. Wang, W., El Hiani, Y., Rubaiy, H. N., and Linsdell, P. (2014) *Relative contribution of different transmembrane segments to the CFTR chloride channel pore.* Pflugers Arch. **466**(3): p. 477-90.
38. Picciotto, M. R., Cohn, J. A., Bertuzzi, G., Greengard, P., and Nairn, A. C. (1992) *Phosphorylation of the cystic fibrosis transmembrane conductance regulator.* J Biol Chem **267**(18): p. 12742-52.
39. Tabcharani, J. A., Chang, X. B., Riordan, J. R., and Hanrahan, J. W. (1991) *Phosphorylation-regulated Cl- channel in CHO cells stably expressing the cystic fibrosis gene.* Nature. **352**(6336): p. 628-31.
40. Corradi, V., P. Vergani, and D.P. Tieleman (2015) *Cystic Fibrosis Transmembrane Conductance Regulator (CFTR): CLOSED AND OPEN STATE CHANNEL MODELS.* J Biol Chem. **290**(38): p. 22891-906.
41. Lewis, H. A., Buchanan, S. G., Burley, S. K., Conners, K., Dickey, M., Dorwart, M., Fowler, R., Gao, X., Guggino, W. B., Hendrickson, W. A. Hunt, J. F., Kearins, M. C., Lorimer, D., Maloney, P. C., Post, K. W., Rajashankar, K. R., Rutter, M. E., Sauder, J. M., Shriver, S., Thibodeau, P. H. Thomas, P. J., Zhang, M., Zhao, X., and Emtage, S. (2004) *Structure of nucleotide-binding domain 1 of the cystic fibrosis transmembrane conductance regulator.* EMBO J. **23**(2): p. 282-93.
42. Mornon, J.P., P. Lehn, and I. Callebaut (2009) *Molecular models of the open and closed states of the whole human CFTR protein.* Cell Mol Life Sci. **66**(21): p. 3469-86.
43. Moody, J. E., Millen, L., Binns, D., Hunt, J. F., and Thomas, P. J. (2002) *Cooperative, ATP-dependent association of the nucleotide binding cassettes during the catalytic cycle of ATP-binding cassette transporters.* J Biol Chem. **277**(24): p. 21111-4.
44. Aleksandrov, L., Aleksandrov, A. A., Chang, X. B., and Riordan, J. R. (2002) *The First Nucleotide Binding Domain of Cystic Fibrosis Transmembrane Conductance Regulator Is a Site of Stable Nucleotide Interaction, whereas the Second Is a Site of Rapid Turnover.* J Biol Chem **277**(18): p. 15419-25.

45. Basso C, Vergani P, Nairn AC, and Gadsby DC. (2003) *Prolonged nonhydrolytic interaction of nucleotide with CFTR's NH2-terminal nucleotide binding domain and its role in channel gating.* J Gen Physiol. **122**(3): p. 333-48.
46. Bai, Y., M. Li, and T.C. Hwang (2011) *Structural basis for the channel function of a degraded ABC transporter, CFTR (ABCC7).* J Gen Physiol. **138**(5): p. 495-507.
47. Cui, G., Rahman, K. S., Infield, D. T., Kuang, C., Prince, C. Z., and McCarty, N. A. (2014) *Three charged amino acids in extracellular loop 1 are involved in maintaining the outer pore architecture of CFTR.* J Gen Physiol. **144**(2): p. 159-79.
48. Wang, W., B.C. Roessler, and K.L. Kirk. (2014) *An electrostatic interaction at the tetrahelix bundle promotes phosphorylation-dependent cystic fibrosis transmembrane conductance regulator (CFTR) channel opening.* J Biol Chem, **289**(44): p. 30364-78.
49. Csanady, L., P. Vergani, and D.C. (2010) Gadsby, *Strict coupling between CFTR's catalytic cycle and gating of its Cl- ion pore revealed by distributions of open channel burst durations.* Proc Natl Acad Sci U S A **107**(3): p. 1241-6.
50. Vergani, P., A.C. Nairn, and D.C. Gadsby (2003) *On the mechanism of MgATP-dependent gating of CFTR Cl- channels.* J Gen Physiol. **121**(1): p. 17-36.
51. Zhou, Y., J.E. Pearson, and A. Auerbach (2005) *Phi-value analysis of a linear, sequential reaction mechanism: theory and application to ion channel gating.* Biophys J. **89**(6): p. 3680-5.
52. Auerbach, A. (2007) *How to turn the reaction coordinate into time.* J Gen Physiol,. **130**(6): p. 543-6.
53. Rudolph A. Marcus. (1968) *Theoretical Relations among Rate Constants, Barriers, and Bronsted Slopes of Chemical Reactions.* J Phys Chem. (78): p. 891-899.
54. Ernest Grunwald, (1985) *Structure-Energy Relations, Reaction Mechanism, and Disparity of Progress of Concerted Reaction Events* .J Am Chem Soc (107): p. 125-133.
55. Csanady, L. (2009) *Application of rate-equilibrium free energy relationship analysis to nonequilibrium ion channel gating mechanisms.* J Gen Physiol. **134**(2): p. 129-36.
56. Segel, I.H. (1993) *Enzyme Kinetics. Behavior and Analysis of Rapid Equilibrium and Steady-State Enzyme Systems.* John Wiley & Sons Inc., New York.
57. Purohit, P., S. Chakraborty, and A. Auerbach (2015) *Function of the M1 pi-helix in endplate receptor activation and desensitization.* J Physiol, **593**(13): p. 2851-66.
58. Purohit, P., Gupta, S., Jadey, S., and Auerbach, A. (2013) *Functional anatomy of an allosteric protein.* Nat Commun **4**: p. 2984.
59. Purohit, P., A. Mitra, and A. Auerbach (2007) *A stepwise mechanism for acetylcholine receptor channel gating.* Nature. **446**(7138): p. 930-3.
60. Mitra, A., G.D. Cymes, and A. Auerbach (2005) *Dynamics of the acetylcholine receptor pore at the gating transition state.* Proc Natl Acad Sci U S A,. **102**(42): p. 15069-74.
61. Aleksandrov, A.A., L. Cui, and J.R. Riordan (2009) *Relationship between nucleotide binding and ion channel gating in cystic fibrosis transmembrane conductance regulator.* J Physiol,. **587**(Pt 12): p. 2875-86.

62. Scott-Ward, T. S., Cai, Z., Dawson, E. S., Doherty, A., Da Paula, A. C., Davidson, H., Porteous, D. J., Wainwright, B. J., Amaral, M. D., Sheppard, D. N., and Boyd, A. C. (2007) *Chimeric constructs endow the human CFTR Cl-channel with the gating behavior of murine CFTR.* Proc Natl Acad Sci U S A. **104**(41): p. 16365-70.
63. Wang, F., Zeltwanger, S., Hu, S., and Hwang, T. C. (2000) *Deletion of phenylalanine 508 causes attenuated phosphorylation-dependent activation of CFTR chloride channels.* J Physiol **524 Pt 3**: p. 637-48.
64. Wang, W., Wu, J., Bernard, K., Li, G., Wang, G., Bevensee, M. O., and Kirk, K. L. (2010) *ATP-independent CFTR channel gating and allosteric modulation by phosphorylation.* Proc Natl Acad Sci U S A **107**(8): p. 3888-93.
65. Zhang, L., Aleksandrov, L. A., Riordan, J. R., and Ford, R. C. (2011) *Domain location within the cystic fibrosis transmembrane conductance regulator protein investigated by electron microscopy and gold labelling.* Biochim Biophys Acta,. **1808**(1): p. 399-404.
66. Miki, H., Zhou, Z., Li, M., Hwang, T. C., and Bompadre, S. G. (2010) *Potentiation of disease-associated cystic fibrosis transmembrane conductance regulator mutants by hydrolyzable ATP analogs.* J Biol Chem. **285**(26): p. 19967-75.
67. Csanady, L. and B. Torocsik (2014) *Catalyst-like modulation of transition states for CFTR channel opening and closing: new stimulation strategy exploits nonequilibrium gating.* J Gen Physiol. **143**(2): p. 269-87.
68. Ishihara, H. and M.J. Welsh (1997) *Block by MOPS reveals a conformation change in the CFTR pore produced by ATP hydrolysis.* Am J Physiol. **273**(4 Pt 1): p. C1278-89.
69. Csanady, L. (2000) *Rapid kinetic analysis of multichannel records by a simultaneous fit to all dwell-time histograms.* Biophys J. **78**(2): p. 785-99.
70. Bompadre, S. G., Ai, T., Cho, J. H., Wang, X., Sohma, Y., Li, M., and Hwang, T. C. (2005) *CFTR gating I: Characterization of the ATP-dependent gating of a phosphorylation-independent CFTR channel (DeltaR-CFTR).* J Gen Physiol,. **125**(4): p. 361-75.
71. Urbatsch, I. L., Beaudet, L., Carrier, I., and Gros, P. (1998) *Mutations in either nucleotide-binding site of P-glycoprotein (Mdr3) prevent vanadate trapping of nucleotide at both sites.* Biochemistry. **37**(13): p. 4592-602.
72. Rai, V., Gaur, M., Shukla, S., Shukla, S., Ambudkar, S. V., Komath, S. S., and Prasad, R. (2006) *Conserved Asp327 of walker B motif in the N-terminal nucleotide binding domain (NBD-1) of Cdr1p of Candida albicans has acquired a new role in ATP hydrolysis.* Biochemistry. **45**(49): p. 14726-39.
73. Hrycyna, C. A., Ramachandra, M., Germann, U. A., Cheng, P. W., Pastan, I., and Gottesman, M. M. (1999) *Both ATP sites of human P-glycoprotein are essential but not symmetric.* Biochemistry. **38**(42): p. 13887-99.
74. Wang, W., He, Z., O'Shaughnessy, T. J., Rux, J., and Reenstra, W. W. (2002) *Domain-domain associations in cystic fibrosis transmembrane conductance regulator.* Am J Physiol Cell Physiol. **282**(5): p. C1170-80.
75. Bozoky, Z., Krzeminski, M., Muhandiram, R., Birtley, J. R., Al-Zahrani, A., Thomas, P. J., Frizzell, R. A., Ford, R. C., and Forman-Kay, J. D. (2013) *Regulatory R region of the CFTR chloride channel is a dynamic integrator of*

phospho-dependent intra- and intermolecular interactions. Proc Natl Acad Sci U S A,. **110**(47): p. E4427-36.

76. Carson, M. R., Travis, S. M., Winter, M. C., Sheppard, D. N., and Welsh, M. J. (1994) *Phosphate stimulates CFTR Cl- channels.* Biophys J,. **67**(5): p. 1867-75.
77. Zeltwanger, S., Wang, F., Wang, G. T., Gillis, K. D., and Hwang, T. C. (1999) *Gating of cystic fibrosis transmembrane conductance regulator chloride channels by adenosine triphosphate hydrolysis. Quantitative analysis of a cyclic gating scheme.* J Gen Physiol,. **113**(4): p. 541-54.
78. Sigworth, F.J. and S.M. Sine (1987) *Data transformations for improved display and fitting of single-channel dwell time histograms.* Biophys J,. **52**(6): p. 1047-54.
79. Magleby, K.L. and B.S. Pallotta (1983) *Burst kinetics of single calcium-activated potassium channels in cultured rat muscle.* J Physiol, **344**: p. 605-23.
80. Cotten, J. F., Ostedgaard, L. S., Carson, M. R., and Welsh, M. J. (1996) *Effect of cystic fibrosis-associated mutations in the fourth intracellular loop of cystic fibrosis transmembrane conductance regulator.* J Biol Chem,. **271**(35): p. 21279-84.
81. Serohijos, A. W., Hegedus, T., Aleksandrov, A. A., He, L., Cui, L., Dokholyan, N. V., and Riordan, J. R. (2008) *Phenylalanine-508 mediates a cytoplasmic-membrane domain contact in the CFTR 3D structure crucial to assembly and channel function.* Proc Natl Acad Sci U S A. **105**(9): p. 3256-61.
82. He, L., Aleksandrov, A. A., Serohijos, A. W., Hegedus, T., Aleksandrov, L. A., Cui, L., Dokholyan, N. V., and Riordan, J. R. (2008) *Multiple membrane-cytoplasmic domain contacts in the cystic fibrosis transmembrane conductance regulator (CFTR) mediate regulation of channel gating.* J Biol Chem. **283**(39): p. 26383-90.
83. Seibert, F. S., Linsdell, P., Loo, T. W., Hanrahan, J. W., Clarke, D. M., and Riordan, J. R. (1996) *Disease-associated mutations in the fourth cytoplasmic loop of cystic fibrosis transmembrane conductance regulator compromise biosynthetic processing and chloride channel activity.* J Biol Chem,. **271**(25): p. 15139-45.
84. Seibert, F. S., Linsdell, P., Loo, T. W., Hanrahan, J. W., Riordan, J. R., and Clarke, D. M. (1996) *Cytoplasmic loop three of cystic fibrosis transmembrane conductance regulator contributes to regulation of chloride channel activity.* J Biol Chem, **271**(44): p. 27493-9.
85. Mornon, J.P., P. Lehn, and I. Callebaut (2008) *Atomic model of human cystic fibrosis transmembrane conductance regulator: membrane-spanning domains and coupling interfaces.* Cell Mol Life Sci **65**(16): p. 2594-612.
86. Zhang, Z.R., S.I. McDonough, and N.A. McCarty (2000) *Interaction between permeation and gating in a putative pore domain mutant in the cystic fibrosis transmembrane conductance regulator.* Biophys J,. **79**(1): p. 298-313.
87. McDonough, S., Davidson, N., Lester, H. A., and McCarty, N. A. (1994) *Novel pore-lining residues in CFTR that govern permeation and open-channel block.* Neuron, **13**(3): p. 623-34.
88. Linsdell, P. (2001) *Relationship between anion binding and anion permeability revealed by mutagenesis within the cystic fibrosis transmembrane conductance regulator chloride channel pore.* J Physiol, **531**(Pt 1): p. 51-66.

89. McCarty, N.A. and Z.R. Zhang (2001) *Identification of a region of strong discrimination in the pore of CFTR.* Am J Physiol Lung Cell Mol Physiol,. **281**(4): p. L852-67.
90. Yeh, H.I., J.T. Yeh, and T.C. Hwang (2015) *Modulation of CFTR gating by permeant ions.* J Gen Physiol,. **145**(1): p. 47-60.
91. Mense, M., Vergani, P., White, D. M., Altberg, G., Nairn, A. C., and Gadsby, D. C. (2006) *In vivo phosphorylation of CFTR promotes formation of a nucleotide-binding domain heterodimer.* EMBO J, **25**(20): p. 4728-39.
92. Chaves, L.A. and D.C. Gadsby (2015) *Cysteine accessibility probes timing and extent of NBD separation along the dimer interface in gating CFTR channels.* J Gen Physiol. **145**(4): p. 261-83.
93. Gao, X. and T.C. Hwang (2015) *Localizing a gate in CFTR.* Proc Natl Acad Sci U S A. **112**(8): p. 2461-6.
94. Csanady, L., A.C. Nairn, and D.C. Gadsby (2006) *Thermodynamics of CFTR channel gating: a spreading conformational change initiates an irreversible gating cycle.* J Gen Physiol. **128**(5): p. 523-33.
95. Jackson, M. B., Wong, B. S., Morris, C. E., Lecar, H., and Christian, C. N. (1983) *Successive openings of the same acetylcholine receptor channel are correlated in open time.* Biophys J **42**(1): p. 109-14.
96. Gunderson, K.L. and R.R. Kopito (1995) *Conformational states of CFTR associated with channel gating: the role ATP binding and hydrolysis.* Cell, **82**(2): p. 231-9.
97. Jih KY, Li M, Hwang TC, and Bompadre SG. (2011) *The most common cystic fibrosis-associated mutation destabilizes the dimeric state of the nucleotide-binding domains of CFTR.* J Physiol **589**(Pt 11): p. 2719-31.
98. Kopeikin Z, Yuksek Z, Yang HY, and Bompadre SG. (2014) *Combined effects of VX-770 and VX-809 on several functional abnormalities of F508del-CFTR channels.* J Cyst Fibros **13**(5): p. 508-14.
99. Winter, M.C. and M.J. Welsh (1997) *Stimulation of CFTR activity by its phosphorylated R domain.* Nature. **389**(6648): p. 294-6.
100. Jih, K.Y. and T.C. Hwang (2013) *Vx-770 potentiates CFTR function by promoting decoupling between the gating cycle and ATP hydrolysis cycle.* Proc Natl Acad Sci U S A **110**(11): p. 4404-9.

DOI:10.14753/SE.2017.2028

10. Candidate's publication

Sorum, B., Czégé, D. & Csanády, L. Timing of CFTR Pore Opening and Structure of Its Transition State. Cell 163, 724-733, doi:http://dx.doi.org/10.1016/j.cell.2015.09.052 (2015).

DOI:10.14753/SE.2017.2028

11. Acknowledgements

I would like to thank Dr. Csanády for giving me this opportunity, from my first year of medical school, to my last year as a PhD student, and hopefully for future collaborations with each other. I would also like to thank Dr. Törőcsik for all her help in molecular biology. The entire ion channel group (Balázs, Iordan, Csaba, and András) for their help over the years. Everyone in the Department of Medical Biochemistry, and to the nation of Hungary, for hosting me for ten years, and allowing me to obtain a world class education. Finally, to my wife who has been patient with me since my first year of medical school.